Cellular Microbiology (2014) **16**(9), 1405–1424

doi:10.1111/cmi.12302
First published online 2 June 2014

The ability of an attaching and effacing pathogen to trigger localized actin assembly contributes to virulence by promoting mucosal attachment

Emily M. Mallick,[1] John J. Garber,[2,3,4] Vijay K. Vanguri,[5] Sowmya Balasubramanian,[6] Timothy Blood,[1] Stacie Clark,[6] Didier Vingadassalom,[1] Christopher Louissaint,[1] Beth McCormick,[1] Scott B. Snapper[2,4,7] and John M. Leong[1,6]***

[1]*Department of Microbiology and Physiological Systems, University of Massachusetts Medical School, 55 Lake Avenue North, Worcester, MA 01655, USA.*
[2]*Division of Gastroenterology/Nutrition & Center for Inflammatory Bowel Disease Treatment and Research, Children's Hospital Boston, Boston, MA 02114, USA.*
[3]*Gastrointestinal Unit, Massachusetts General Hospital, Harvard Medical School, Boston, MA 02114, USA.*
[4]*Department of Medicine, Harvard Medical School, Boston, MA 02115, USA.*
[5]*Department of Pathology, University of Massachusetts Medical School, Worcester, MA 01655, USA.*
[6]*Department of Molecular Biology and Microbiology, Tufts University School of Medicine, 136 Harrison Avenue, Boston, MA 02111, USA.*
[7]*Division of Gastroenterology & Hepatology, Brigham & Women's Hospital, Boston, MA 02115, USA.*

Summary

Enterohaemorrhagic *Escherichia coli* (EHEC) colonizes the intestine and causes bloody diarrhoea and kidney failure by producing Shiga toxin. Upon binding intestinal cells, EHEC triggers a change in host cell shape, generating actin 'pedestals' beneath bound bacteria. To investigate the importance of pedestal formation to disease, we infected genetically engineered mice incapable of supporting pedestal formation by an EHEC-like mouse pathogen, or wild type mice with a mutant of that pathogen incapable of generating pedestals. We found that pedestal formation promotes attachment of bacteria to the intestinal mucosa and vastly increases the severity of Shiga toxin-mediated disease.

Received 19 February, 2014; revised 9 April, 2014; accepted 13 April, 2014. For correspondence. *E-mail john.leong@tufts.edu; Tel. (+1) 617 636 0488; Fax (+1) 617 636 0337; **E-mail Scott.Snapper@childrens.harvard.edu; Tel. (+1) 617 919 4973; Fax (+1) 617 730 0498.

Dedication: This work is dedicated to the memory of David Schauer, who was critical to its initiation.

Introduction

Enterohaemorrhagic *Escherichia coli* (EHEC), particularly serotype O157:H7, is an important food-borne pathogen responsible for outbreaks of human diarrhoeal disease (Kaper *et al.*, 2004; Pennington, 2010). EHEC infection can present as haemorrhagic colitis, as well as a life-threatening systemic disease known as haemolytic uraemic syndrome (HUS), characterized by haemolytic anaemia, thrombocytopenia, and renal failure (Tarr *et al.*, 2005; Karmali *et al.*, 2009). HUS is the leading cause of renal failure in children (Scheiring *et al.*, 2008).

Systemic disease resulting from EHEC infection requires production of a phage-encoded Shiga toxin (Stx) (Schmidt, 2001). Stx produced in the gut traverses the intestinal epithelium, enters the bloodstream, and targets organs expressing the globotriaosylceramide Gb_3 receptor, including the vasculature, kidneys, and central nervous system (Obrig, 2010; Schuller, 2011), where it inhibits protein synthesis. Of Stx1 and Stx2, the two major serotypes of Stx, EHEC strains that produce only Stx2 are associated with a greater risk of HUS (Croxen and Finlay, 2010; Melton-Celsa *et al.*, 2011).

A distinctive colonization feature of EHEC that it shares with enteropathogenic *E. coli*, a cause of infantile diarrhoea in the developing world, and *Citrobacter rodentium*, a closely related murine pathogen that causes colonic hyperplasia, is the ability to form attaching and effacing (AE) lesions on the intestinal epithelium (Schauer and Falkow, 1993a; Kaper *et al.*, 2004). AE lesions are characterized by the effacement of brush border microvilli, intimate attachment of bacteria to the host cell, and the formation of actin 'pedestals' beneath bound bacteria (Moon *et al.*, 1983; Kaper *et al.*, 2004). Upon animal infection with EHEC or *C. rodentium*, mucosally adhered bacteria and AE lesions have been observed in the caecum, an initial site of colonization of mice by *C. rodentium*,

colon, and rectum (Schauer and Falkow, 1993a; Dean-Nystrom *et al*., 1999; Wales *et al*., 2001; Nagano *et al*., 2003; Wiles *et al*., 2004; Nart *et al*., 2008). The relationship between two central features of EHEC pathogenesis, i.e. AE lesion formation and Stx-mediated disease, is relatively unexplored.

AE lesion formation is dependent on a type III secretion system (T3SS) that translocates bacterial effectors into host cells (McDaniel *et al*., 1995; Garmendia *et al*., 2005). Tir (translocated intimin receptor) is essential for pedestal formation and localizes to and spans the host cell plasma membrane. The extracellular domain of Tir binds to the bacterial outer membrane protein intimin (Kenny *et al*., 1997; de Grado *et al*., 1999; Hartland *et al*., 1999), which then induces Tir clustering and the formation of actin pedestals in a process dependent on the host cell protein N-WASP (reviewed in Caron *et al*., 2006; Hayward *et al*., 2006; Campellone, 2010). For *C. rodentium* and EPEC Tir, the region critical for pedestal induction includes a tyrosine residue [TirY471 in *C. rodentium*, TirY474 in EPEC (Kenny, 1999; Gruenheid *et al*., 2001; Campellone *et al*., 2002)] that is phosphorylated by mammalian cell kinases (Phillips *et al*., 2004; Swimm *et al*., 2004), creating a docking site for the host cell adaptor protein Nck (Gruenheid *et al*., 2001; Campellone *et al*., 2002; 2004a). Nck recruits N-WASP, which, when activated, interacts with the Arp 2/3 actin nucleating complex and strongly stimulates localized actin polymerization beneath adherent bacteria (Rohatgi *et al*., 2001; Rivera *et al*., 2004; Frankel and Phillips, 2008). Although EHEC strains produce Tir and intimin, canonical EHEC Tir lacks a Nck binding sequence and instead translocates into host cells an additional bacterial factor, $EspF_U$ (aka TccP) (Campellone *et al*., 2004b; Garmendia *et al*., 2004) which independently binds N-WASP and drives actin assembly via a Nck-independent pathway (Campellone and Leong, 2005; Brady *et al*., 2007). Interestingly, these two distinct actin polymerization signalling pathways are not absolute: some EPEC and EHEC strains possess redundant mechanisms of actin polymerization (Whale *et al*., 2006; Ogura *et al*., 2007).

While intimin and Tir are required for efficient host cell binding and for colonization in animal models (Donnenberg *et al*., 1993; Schauer and Falkow, 1993b; Tzipori *et al*., 1995; Marches *et al*., 2000; Deng *et al*., 2003; Ritchie *et al*., 2003), a number of studies have found that the specific ability of Tir to trigger actin assembly is dispensable for colonization. For example, murine infection with a 'pedestal-defective' *C. rodentium* strain (i.e. one that cannot trigger efficient pedestal formation on cultured mammalian cells) was not significantly attenuated for intestinal colonization compared to infection by a pedestal-competent strain (Deng *et al*., 2003). Similarly, faecal shedding in calves and lambs was unaltered upon infection with an EHEC pedestal-defective mutant (Vlisidou *et al*., 2006), and colonization of human intestinal explants by EPEC Tir phosphorylation-deficient mutants was similar to that of wild type, pedestal-competent EPEC strains (Schuller *et al*., 2007a).

In contrast, several studies have suggested that the ability to trigger actin pedestals may promote colonization. For example, compared to wild type strains, an EHEC pedestal-defective strain displayed a mild colonization defect late in infection of infant rabbits and generated smaller bacterial aggregates on the intestinal mucosa of gnotobiotic piglets (Ritchie *et al*., 2008). In addition, although a *C. rodentium* pedestal-defective mutant did not show a significant colonization defect during single infection, this strain was outcompeted by wild type *C. rodentium* during co-infection (Crepin *et al*., 2010).

Investigation of the role of AE lesion formation in systemic disease by EHEC has been limited by the lack of model systems that prominently manifest Stx-mediated systemic disease. We recently described a murine infection model utilizing a *C. rodentium* strain lysogenized with the Stx-producing phage Φ1720a-02 [herein referred to as '*C. rodentium* (Φstx_{2dact})'], which induces AE lesion formation, intestinal damage and renal compromise, similar to EHEC toxin-mediated disease (Mallick *et al*., 2012b). We infected a murine host defective in pedestal formation with either non-toxigenic *C. rodentium* or *C. rodentium* (Φstx_{2dact}), and a wild type murine host with mutants of *C. rodentium* or *C. rodentium* (Φstx_{2dact}) that are incapable of robust pedestal formation. Our results revealed that the ability of the AE pathogen to trigger localized actin assembly contributes to virulence by promoting mucosal attachment, particularly in the colon.

Results

Mice devoid of intestinal N-WASP do not permit AE pathogen-induced pedestal formation or mucosal colonization

To determine the requirement for pedestal formation for colonization by AE pathogens, we generated mice deficient in N-WASP, a host protein required for AE pathogen-induced actin pedestal assembly. Since germline deletion of N-WASP results in early embryonic lethality (Lommel *et al*., 2001; Snapper *et al*., 2001), we generated mice specifically devoid only of intestinal N-WASP (i.e. iNWKO mice). Western blot analysis confirmed that N-WASP was expressed in the colon, ileum, and jejunum of littermate control mice (designated 'LMC' in figures), but was absent from these sites in iNWKO mice (Fig. 1A). iNWKO mice were viable but gained weight less rapidly than their

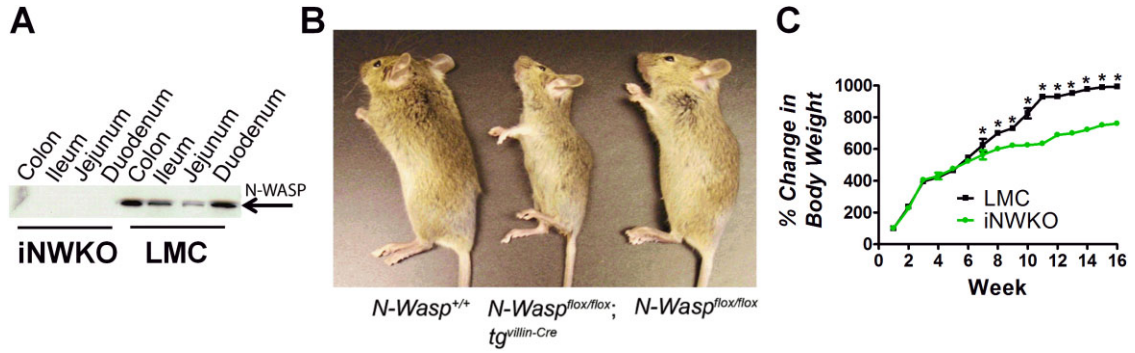

Fig. 1. Mice deleted for intestinal N-WASP are viable and fertile but gain less weight than littermate controls.
A. Western blot analysis of N-WASP expression in intestinal tissue from 8-week-old iNWKO and littermate control mice confirmed complete deletion of N-WASP throughout the small and large intestine. Tubulin was used as a loading control.
B. Appearance of wild type (*N-Wasp*$^{+/+}$), iNWKO (*N-Wasp*$^{flox/flox}$ *tg*$^{vil\text{-}Cre}$), and littermate control (*N-Wasp*$^{flox/flox}$) mice at 12 weeks.
C. Mean change in body weight over time, ± SEM, of iNWKO and littermate control mice. Data represent five mice per group. Black squares: littermate control mice. Green circles: iNWKO mice. The asterisk (*) indicates a statistical difference between iNWKO and littermate control mice as determined by two-way ANOVA followed by Bonferroni post-tests ($P < 0.05$).

littermate controls (Fig. 1B and C), specifically between eight and 15 weeks of age (Fig. 1C). Histological examination of intestinal tissue from iNWKO mice revealed grossly normal crypt-villous architecture and the presence of all epithelial cell lineages (Fig. S1). Although iNWKO mice displayed abnormal microvilli and decreased perijunctional actin, there was no evidence of spontaneous inflammation, neutrophilic infiltrate, or increased cellularity of the lamina propria (Fig. S1).

To determine if colonization was dependent on intestinal N-WASP, iNWKO and littermate control mice were infected for 7 days with approximately 5×10^8 cfu of GFP-*C. rodentium* (see Table S1). Despite repeated attempts, mucosal colonization of the colons of iNWKO mice, in contrast to littermate controls, was insufficient to permit reliable assessment AE lesions by transmission electron microscopy (TEM) (data not shown). Therefore, we evaluated colonic mucosal-association of *C. rodentium* using immunofluorescent (IF) analyses. Whereas the colonic mucosa of infected littermate controls revealed large numbers of bound bacteria, no mucosal-associated bacteria were detected in the colons of infected iNWKO mice (Fig. 2A and B).

To further evaluate colonization by *C. rodentium* in the absence of N-WASP, faecal shedding was assessed in iNWKO and littermate control mice by quantifying bacterial cfu g^{-1} stool. Faecal shedding in iNWKO mice was ~ 100-fold lower than in littermate control mice at 7 days post-infection (Fig. 2C). In contrast, oral infection of iNWKO mice by another intestinal pathogen, *Salmonella enterica*, resulted in intestinal colonization with concomitant inflammatory changes in the mucosa indistinguishable from that of littermate controls (Fig. S2A, D and E). Together, these data indicate that N-WASP is required for intestinal colonization by *C. rodentium*.

N-WASP promotes high-level colonization and systemic disease during toxigenic C. rodentium *infection*

To determine whether the N-WASP pathway of actin pedestal formation was required for high-level faecal

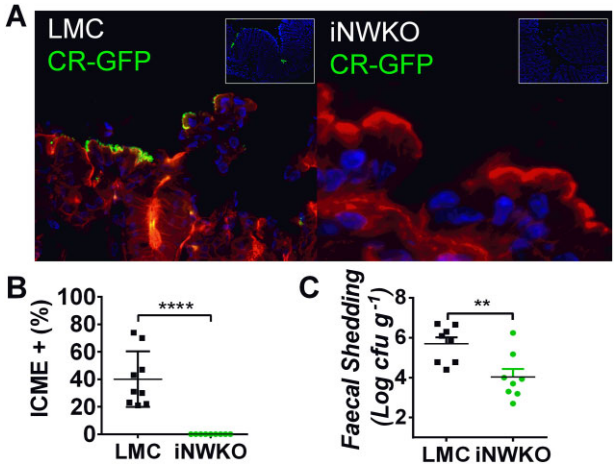

Fig. 2. Intestinal N-WASP is required for colonization of mice by *C. rodentium*.
A. Littermate control and iNWKO mice were infected with 5×10^8 GFP-*C. rodentium* by oral gavage. At 4 days post-infection, after DAPI-staining (blue) to visualize intestinal cells and phalloidin-staining (red) to visualize the cell architecture, large numbers of adherent GFP-positive *C. rodentium* were identified in littermate control mice (left panel) but not iNWKO mice (right panel). Inset shows low power view of DAPI and GFP, indicating the absence of identifiable *C. rodentium* in iNWKO mice.
B. Intercrypt mucosal epithelium (ICME) with adherent GFP+ *C. rodentium* was quantified in littermate control and iNWKO mice at 4 days post-infection. Shown is the mean ± SD. Statistical significance was determined by unpaired *t*-test and $^{****}P < 0.0001$.
C. Faecal shedding (± SEM) of iNWKO or littermate control mice at 7 days post-infection by *C. rodentium* was determined by quantifying viable stool counts. Data reflect a compilation of two experiments, with a total of four mice per group per experiment. ($^{**}P < 0.01$; by an unpaired *t*-test.)

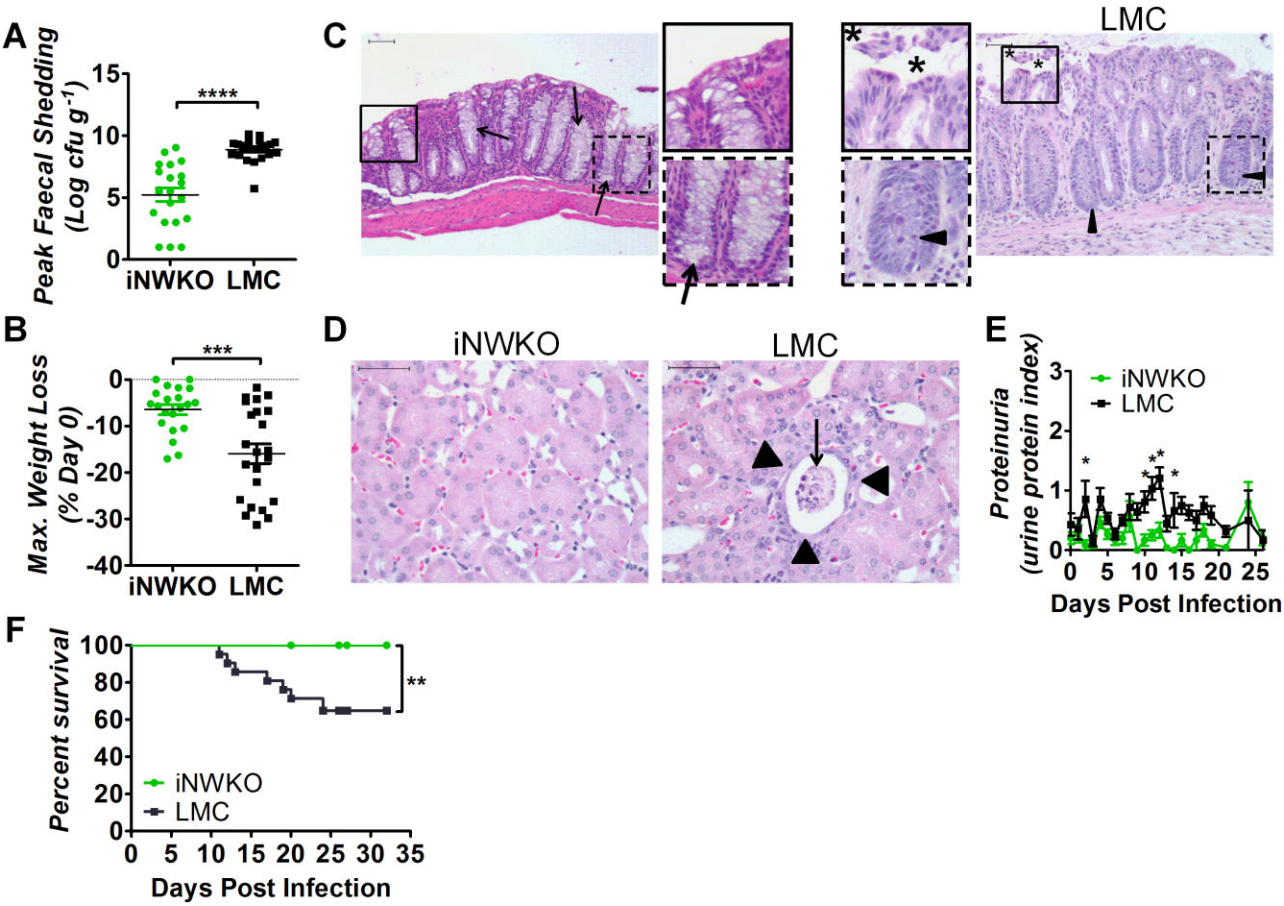

Fig. 3. N-WASP promotes high-level colonization and systemic disease during *C. rodentium* (Φstx_{2dact}) infection.
A. Faecal shedding by iNWKO or littermate control mice infected with *C. rodentium* (Φstx_{2dact}) shown as peak cfu (± SEM) of 21 iNWKO and 22 littermate controls from a compilation of five experiments. (****$P < 0.0001$ by unpaired *t*-test.)
B. Maximum percent body weight loss during infection of iNWKO or littermate control mice infected with *C. rodentium* (Φstx_{2dact}) (± SEM) of 21 iNWKO and 23 littermate controls from a compilation of five experiments. (***$P < 0.001$ by unpaired *t*-test.)
C and D. H&E-stained intestinal (C) and kidney (D) sections of iNWKO and littermate control mice infected with *C. rodentium* (Φstx_{2dact}) at 11 days post-infection. Scale bars measure 50 μm. Insets: magnification of original images. (C) Asterisks indicate disrupted and sloughed intestinal mucosa. Arrowheads and arrows indicate inflammation and goblet cells respectively. Magnification, 200×. (D) Arrowheads indicate flattened tubule lining and arrows indicate sloughed tubules and necrotic tissue. Magnification, 400×.
E. Urine protein content, represented as average protein index (± SEM), in iNWKO and littermate control mice infected with *C. rodentium* (Φstx_{2dact}). Data are a compilation of three experiments, comprising a total of 15 iNWKO and 16 littermate control mice. (*$P < 0.05$ by repeated measures two-way ANOVA followed by Bonferroni post-tests; in addition, as described in *Experimental procedures*, the return of average proteinuria towards baseline depicted in the graph preceded clinical recovery of individual mice by a few days.)
F. Percent survival of iNWKO and littermate control mice infected with *C. rodentium* (Φstx_{2dact}). Data represent a compilation of five experiments, comprising a total of 19 iNWKO mice and 21 littermate control mice. Statistical significance was determined using a Log-rank (Mantel-Cox) Test, revealing a significant ($P < 0.01$) difference between the two groups.

shedding upon infection with toxigenic *C. rodentium*, iNWKO and littermate control mice were infected with approximately 1×10^9 cfu *C. rodentium* (Φstx_{2dact}) by oral gavage. Viable stool counts throughout infection showed that faecal shedding in littermate controls reached a peak of approximately 10^9 cfu g^{-1} stool between 11 and 14 days post-infection and slowly diminished thereafter (Fig. 3A and Fig. S3A). By 30 days post-infection, bacteria were no longer detected in the stool, as previously observed in immunocompetent mice (Fig. S3A; Ghaem-Maghami *et al.*, 2001; Vallance *et al.*, 2002; Simmons *et al.*, 2003). In contrast, average peak faecal shedding of *C. rodentium* (Φstx_{2dact}) by iNWKO mice was dramatically diminished (Fig. 3A) and bacteria were absent in stool by 30 days post-infection (Fig. S3A).

Weight loss is common in murine models of HUS (Mohawk and O'Brien, 2011; Mallick *et al.*, 2012b). N-WASP-proficient littermate controls infected with *C. rodentium* (Φstx_{2dact}) maintained body weight through 9 days post-infection, but lost significant weight, averaging 15.5%, thereafter (Fig. 3B and Fig. S3B). Maximal weight loss typically occurred at peak colonization or just prior to

euthanasia due to the deteriorating condition of the animals (Fig. 3B). Mice that did not succumb to lethal disease regained body weight as faecal counts diminished to zero by approximately 25 days post-infection (Fig. S3B). In contrast, body weight of iNWKO mice remained constant throughout the course of infection (Fig. 3B and Fig. S3B).

As intestinal damage is often observed in patients with HUS and in murine infection by *C. rodentium* (Φstx_{2dact}) (Mallick *et al*., 2012b), intestinal sections of iNWKO mice and littermate control mice infected with *C. rodentium* (Φstx_{2dact}) were examined histologically. Littermate control intestines displayed severe damage to the mucosal surface, infiltration of inflammatory cells, crypt withering, and depletion of goblet cells (Fig. 3C), all evidence of acute injury. In contrast, the intestines of iNWKO mice appeared histologically normal.

Renal damage, a hallmark of Stx-mediated disease, was evaluated both histologically and functionally in iNWKO and littermate control mice infected with *C. rodentium* (Φstx_{2dact}). N-WASP-proficient littermate control mice showed severe proximal tubular damage, with sloughed cells in the lumen and flattening of the epithelium (Fig. 3D). Mitotic activity was observed in some proximal tubule cells, presumably reflecting regeneration of damaged cells (V.K. Vanguri and E.M. Mallick, unpubl. obs.). This renal pathology corresponded to functional compromise, as littermate control mice developed significant proteinuria, specifically early in infection and at time points corresponding to peak faecal shedding, i.e. at approximately 10 days post-infection (Fig. 3E). In contrast, the kidneys of iNWKO mice showed no evidence of histological damage, and protein was not detected in the urine (Fig. 3D and E). The absence of systemic damage to iNWKO mice infected with *C. rodentium* (Φstx_{2dact}) was specific to that enteric pathogen, as *Salmonella*-infected iNWKO mice suffered hepatic and splenic colonization and damage indistinguishable from littermate controls (Fig. S2B, C and E).

The absence of weight loss, intestinal damage, and kidney dysfunction in infected iNWKO mice corresponded to 100% survival (Fig. 3F). In contrast, approximately 35% of littermate control mice infected with *C. rodentium* (Φstx_{2dact}) succumbed to lethal disease (Fig. 3F). These data indicate that N-WASP, a host factor critical for pedestal formation, is required for Stx-mediated weight loss, intestinal and renal damage, and lethality after infection with *C. rodentium* (Φstx_{2dact}).

C. rodentium *Tir-mediated actin assembly promotes colonization of the colonic mucosa*

Mice specifically deficient for intestinal N-WASP displayed changes in microvillar architecture and junctional integrity (data not shown) that could contribute in unpredictable ways to differences in responses to *C. rodentium* infection. In addition, N-WASP has been shown to increase effector translocation (Vingadassalom *et al*., 2010) a process necessary for efficient colonization (Deng *et al*., 2004; Ritchie and Waldor, 2005), so the colonization defect observed in the iNWKO mice may partially be due to diminished type III translocation. Therefore, we also examined the role of pedestal formation in intestinal colonization by utilizing a bacterial *tir* point mutant defective for pedestal formation. We generated plasmid, $pTir_{Y471F}$, encoding *C. rodentium* TirY471F that, despite promoting attachment to cultured cells, does not promote pedestal formation *in vitro* because of the lack of the tyrosine residue critical for Nck recruitment (Deng *et al*., 2003; Crepin *et al*., 2010). An equivalent tyrosine to phenylalanine substitution in EPEC Tir gave rise to a similar phenotype in EPEC (Schuller *et al*., 2007a). Western blot analysis of bacterial pellets and culture supernatants revealed that *C. rodentium*Δ*tir* (Mallick *et al*., 2012a) harbouring $pTir_{Y471F}$ produced and secreted levels of Tir indistinguishable from an isogenic strain harbouring $pTir_{WT}$ (Mallick *et al*., 2012b) (Fig. S4A and B).

As previously shown (Deng *et al*., 2003; Crepin *et al*., 2010; Mallick *et al*., 2012b), whereas mice infected with wild type *C. rodentium* shed high levels of bacteria in the faeces (Fig. 4A), those infected with *C. rodentium*Δ*tir* displayed faecal counts below the limit of detection (< 100 cfu g^{-1} faeces; data not shown). $pTir_{WT}$ significantly, but partially, complemented the faecal shedding defect of *C. rodentium*Δ*tir*, with slightly delayed kinetics (Fig. 4A), similar to complementation by plasmid-encoded Tir in other studies (Deng *et al*., 2003; Mallick *et al*., 2012b). Consistent with partial complementation by pTir, TEM of the colonic mucosa revealed very few bound *C. rodentium*Δ*tir*/$pTir_{WT}$ (data not shown), although IF staining, which samples larger areas, readily revealed bound bacteria (see below). Approximately a third of recovered faecal bacteria lost the Tir-encoding plasmid (Table S4), likely contributing to the partial nature of the complementation. $pTir_{Y471F}$ also partially complemented *C. rodentium*Δ*tir* for faecal shedding, although to a somewhat lesser degree than $pTir_{WT}$ (Fig. 4A). An analysis of multiple experiments confirmed that peak faecal shedding (i.e. the single-highest titre of faecal cfu observed during the course of infection) by mice infected with *C. rodentium*Δ*tir*/$pTir_{Y471F}$ was approximately threefold lower than by mice infected with *C. rodentium*Δ*tir*/$pTir_{WT}$ ($P = 0.0121$; Fig. 4B, Table 1). This result could not be attributed to a differential loss of $pTir_{WT}$ and $pTir_{Y471F}$, as both plasmids were retained by *C. rodentium*Δ*tir* to the same degree throughout infection (Table S4).

Citrobacter rodentium initiates infection in the murine caecum, then spreads to the colon after several days

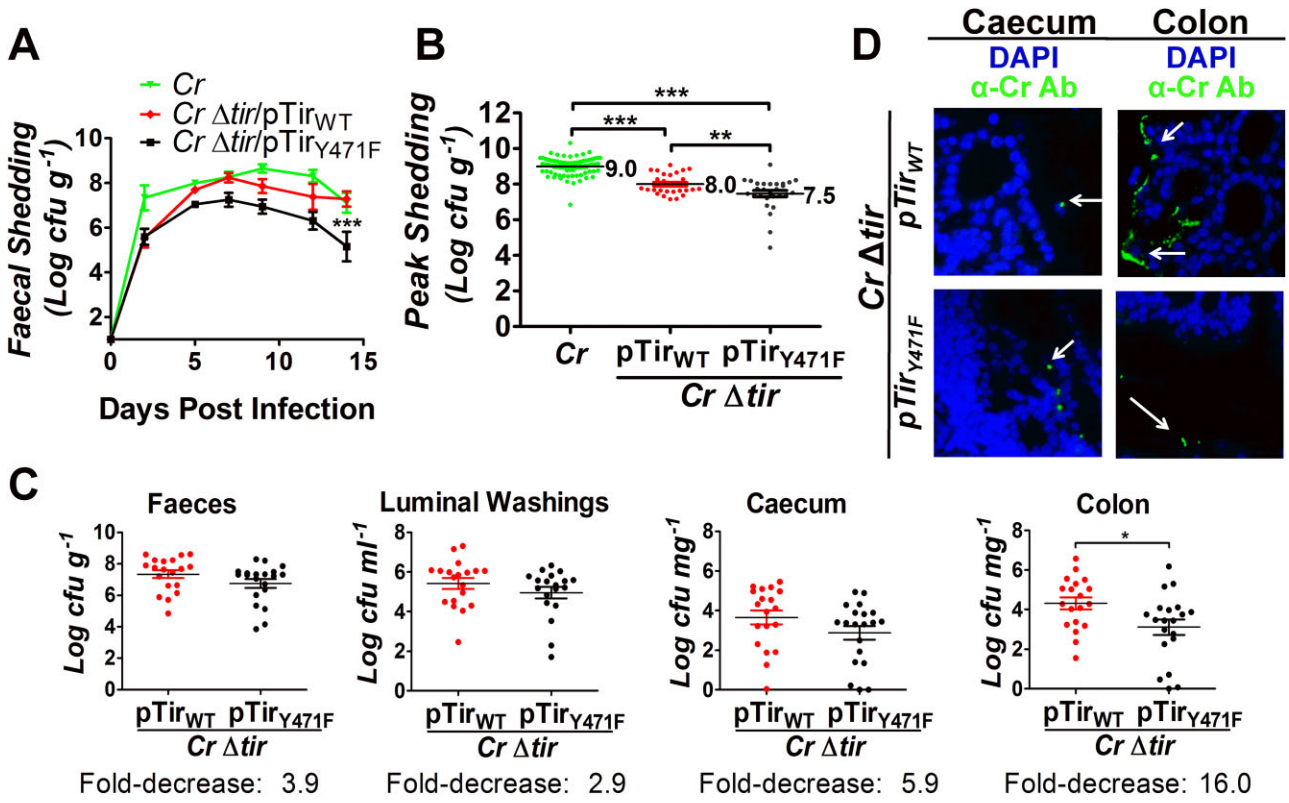

Fig. 4. Tir-mediated actin assembly by *C. rodentium* promotes colonization of the colonic mucosa.
A. Faecal shedding by mice infected with the indicated strain was determined. Data represent the mean cfu (± SEM) from groups of five mice in one of six experiments. '***' ($P < 0.01$, by repeated measures two-way ANOVA followed by Bonferroni post-tests) indicates a statistically significant difference from *C. rodentium* or *C. rodentium*Δ*tir*/pTir$_{WT}$.
B. Mean peak faecal shedding by mice infected with the indicated strain ± SEM. Data are a compilation of 14 experiments for wild type *C. rodentium* and five experiments for *C. rodentium*Δ*tir*/pTir$_{WT}$ or *C. rodentium*Δ*tir*/pTir$_{Y471F}$. Each data point represents an individual mouse. Log mean peak faecal shedding is given to the right of each set. (**$P < 0.01$; ***$P < 0.001$.)
C. Faecal shedding by mice infected with *C. rodentium*Δ*tir*/pTir$_{WT}$ and *C. rodentium*Δ*tir*/pTir$_{Y471F}$ at 6 days post-infection (left panel). Luminal colonization was measured by determining cfu ml^{-1} of luminal washings (second panel). Intestinal colonization (caecal and colonic) was measured by determining cfu mg^{-1} of tissue homogenate (right two panels). Depicted is a compilation of four individual experiments with 3–10 mice per group. Each data point represents an individual mouse. Horizontal line indicates the mean, and fold decrease in colonization by *C. rodentium*Δ*tir*/pTir$_{Y471F}$ compared with *C. rodentium*Δ*tir*/pTir$_{WT}$ is shown below. Error bars indicate ± SEM. (*$P < 0.05$.)
D. Caecal and colonic sections of mice infected with the indicated strain were taken at 6 days post-infection and were stained with DAPI (blue) and anti-*Citrobacter* antibody (green). For these mice, faecal shedding of bacterial strains was equivalent (1.1×10^7 g^{-1} and 2.8×10^7 g^{-1} for *C. rodentium*Δ*tir*/pTir$_{WT}$ and *C. rodentium*Δ*tir*/pTir$_{Y471F}$, respectively, for the caecal sections, and 2.8×10^7 g^{-1} and 1.1×10^7 g^{-1} for *C. rodentium*Δ*tir*/pTir$_{WT}$ and *C. rodentium*Δ*tir*/pTir$_{Y471F}$ respectively for the colonic sections). Magnification: 600×. White arrows indicate bacteria.

(Wiles *et al.*, 2004). To determine if actin pedestal formation is particularly important to colonization of a specific intestinal segment, mice infected with either *C. rodentium*Δ*tir*/pTir$_{WT}$ or *C. rodentium*Δ*tir*/pTir$_{Y471F}$ were euthanized and necropsied at the approximate peak of faecal shedding (i.e. 6 days post-infection). We quantified bacteria in luminal washings, as well as caecum- or colon-associated bacteria retained after removal of faeces and

Table 1. Enhanced faecal shedding is associated with the ability to generate actin pedestals and with lysogeny by Φ*stx*$_{2dact}$.

Parental strain	Log peak faecal shedding			Shedding defect of pTir$_{Y471F}$ vs. pTir$_{WT}$ (*P*-value)
	WT	Δ*tir*/pTir$_{WT}$	Δ*tir*/pTir$_{Y471F}$	
C. rodentium	9.0 (± 0.05) ($n = 82$)	8.0 (± 0.11) ($n = 28$)	7.5 (± 0.17) ($n = 28$)	3.2-fold ($P = 0.0121$)
C. rodentium (Φ*stx*$_{2dact}$)	9.8 (± 0.04) ($n = 132$)	8.8 (± 0.17) ($n = 39$)	8.1 (± 0.14) ($n = 20$)	5.0-fold ($P = 0.0082$)
Increase associated with Φ*stx*$_{2dact}$ (*P*-value)	6.3-fold ($P < 0.0001$)	6.3-fold ($P = 0.0008$)	4.0-fold ($P = 0.0172$)	

n = number indicates the number of mice infected with the designated strain, and is a compilation of results from four or more experiments. P = *P*-value by two-tailed, unpaired Student's *t*-test.

Table 2. The ability to generate actin pedestals is associated with colonization of the colonic mucosa.

	% positive caecal samples[a]		% positive colonic samples	
Strain harbouring plasmid	$pTir_{WT}$	$pTir_{Y471F}$	$pTir_{WT}$	$pTir_{Y471F}$
*C. rodentium*Δ*tir*	53% (9/17[b])	12%[c] (2/17)	53% (9/17)	0%[c] (0/17)
*C. rodentium*Δ*tir* (Φ*stx*$_{2dact}$)	72% (13/18)	26%[c,d] (5/19)	72% (13/18)	0%[c] (0/19)

a. Intestinal samples with bacteria adherent to the epithelium were scored positive (see *Experimental procedures*).
b. Denotes the number of mice with samples positive for mucosally adherent bacteria divided by the total number of mice analysed.
c. The percentage of positive samples was significantly ($P < 0.05$ by Student's *t*-test) less than that found for the isogenic strain producing wild type Tir infecting the corresponding intestinal segment.
d. The percentage of positive caecal samples was significantly ($P < 0.05$ by Student's *t*-test) greater than that found for the identical strain infecting the colon.

luminal washings. In luminal washings, *C. rodentium*Δ*tir*/$pTir_{Y471F}$ was present at approximately threefold lower levels than *C. rodentium*Δ*tir*/$pTir_{WT}$, similar to the approximately fourfold lower levels of *C. rodentium*Δ*tir*/$pTir_{Y471F}$ found in faeces (Fig. 4C, first and second panels). Similarly, *C. rodentium*Δ*tir*/$pTir_{Y471F}$ was present in caecal homogenates at approximately sixfold lower levels than bacteria producing *C. rodentium*Δ*tir*/$pTir_{WT}$ (Fig. 4C, third panel). None of the above differences in bacterial counts reached statistical significance. However, in contrast, *C. rodentium*Δ*tir*/$pTir_{Y471F}$ displayed a significant ~ 16-fold reduction in colonic colonization compared with *C. rodentium*Δ*tir*/$pTir_{WT}$ (Fig. 4C, fourth panel).

We next used IF staining to localize the association of pedestal-competent (*C. rodentium*Δ*tir*/$pTir_{WT}$) and pedestal-defective (*C. rodentium*Δ*tir*/$pTir_{Y471F}$) bacteria with the mucosal surfaces of the caecum and colon during infection near peak faecal shedding (when the faecal concentrations of the two bacterial strains were similar). Randomly chosen caecal samples from each infected mouse were visually scored (*Experimental procedures*), revealing that 53% of mice (9/17) infected with *C. rodentium*Δ*tir*/$pTir_{WT}$ were positive for mucosal attachment, whereas 12% of caecal specimens (2/17) from mice infected with *C. rodentium*Δ*tir*/$pTir_{Y471F}$ were positive ($P < 0.01$; Fig. 4D; Table 2). These results were consistent with our finding that caecal homogenates contained approximately sixfold fewer *C. rodentium*Δ*tir*/$pTir_{Y471F}$ cfu than *C. rodentium*Δ*tir*/$pTir_{WT}$ (Fig. 4C). In the colon, none of the 17 mice infected with *C. rodentium*Δ*tir*/$pTir_{Y471F}$ displayed mucosally attached bacteria (Fig. 4D), compared with 53% of mice (9/17) infected with the pedestal-competent strain ($P < 0.001$; Table 2), consistent with the more severe (~ 16-fold) colonic colonization defect seen with pedestal-defective *C. rodentium* (Fig. 4C).

Tir-mediated actin assembly by C. rodentium *(Φ*stx$_{2dact}$*) promotes colonization of the colonic mucosa*

Stx is essential for systemic disease (Mohawk and O'Brien, 2011; Mallick *et al*., 2012b) and, additionally, promotes EHEC colonization in a murine model (Robinson *et al*., 2006). We previously noted that *C. rodentium* (Φ*stx*$_{2dact}$) exhibited an approximately 3- to 10-fold enhancement of faecal shedding compared with the non-lysogenic *C. rodentium* parental strain, but this difference did not reach statistical significance using experimental groups of five mice (Mallick *et al*., 2012b). We therefore pooled multiple experiments encompassing many (i.e. > 250) mice and found that peak faecal shedding of *C. rodentium* (Φ*stx*$_{2dact}$) was approximately sixfold higher ($P < 0.0001$) than that of the parental non-lysogenic *C. rodentium* strain (Table 1). Lysogeny by Φ*stx*$_{2dact}$ did not appear to alter the kinetics of infection, as peak faecal shedding occurred at ~ 6–8 days post-infection for both strains (Mallick *et al*., 2012b).

We further found that *C. rodentium* (Φ*stx*$_{2dact}$)Δ*tir*/$pTir_{WT}$ and *C. rodentium* (Φ*stx*$_{2dact}$)Δ*tir*/$pTir_{Y471F}$ produced and secreted similar levels of Tir (Fig. S4C and D) and bound indistinguishably to cultured murine cells. On average, each mammalian cell bound 6.89 ± 0.62 versus 6.50 ± 1.7 bacteria for $pTir_{WT}$ and $pTir_{Y471F}$ strains, respectively (Fig. S5A), despite the inability of *C. rodentium* (Φ*stx*$_{2dact}$)Δ*tir*/$pTir_{Y471F}$ to generate actin pedestals on cultured cells (Fig. S5B). Tir was clearly required for efficient binding, as mammalian cells bound an average of only 0.04 Tir-deficient bacteria.

We next sought to evaluate the importance of pedestal formation on murine colonization by Stx-producing *C. rodentium*. As mentioned above, infection with *C. rodentium* (Φ*stx*$_{2dact}$) resulted in high-level faecal shedding, peaking at approximately 7 days post-infection, whereas faecal shedding of *C. rodentium* (Φ*stx*$_{2dact}$)Δ*tir* was below detectable levels (< 100 cfu g^{-1} faeces) (Mallick *et al*., 2012b; Table 1). Complementation of *C. rodentium* (Φ*stx*$_{2dact}$)Δ*tir* with $pTir_{WT}$ restored faecal shedding, albeit at lower levels and with delayed kinetics compared with wild type *C. rodentium* (Φ*stx*$_{2dact}$), consistent with previous results suggesting that plasmid-based complementation of *C. rodentium* (Φ*stx*$_{2dact}$)Δ*tir* is incomplete (Mallick *et al*., 2012b; Fig. 5A; Table 1). *C. rodentium* (Φ*stx*$_{2dact}$)Δ*tir*/$pTir_{Y471F}$ displayed further diminished faecal

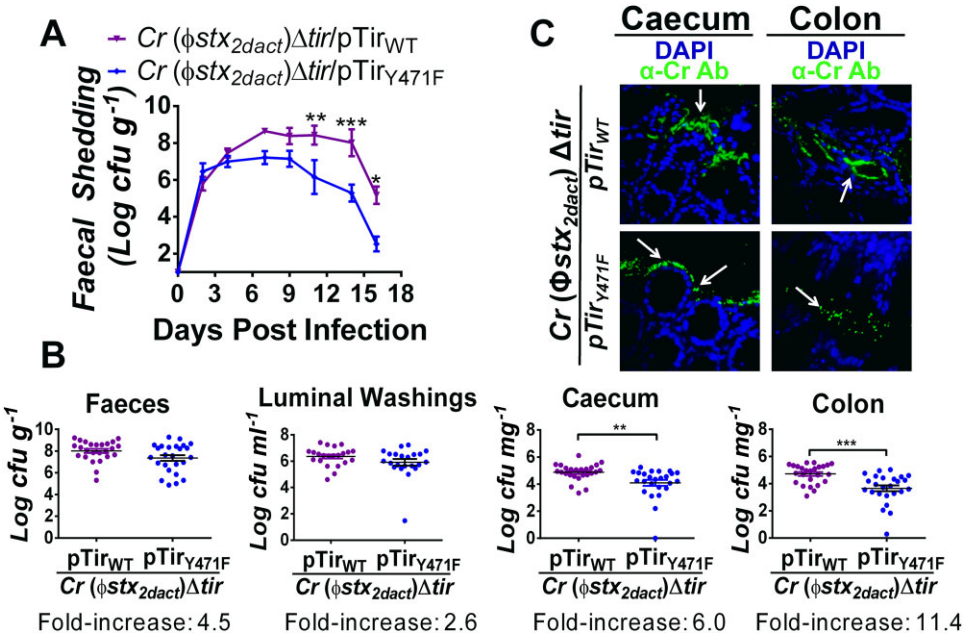

Fig. 5. Tir-mediated actin assembly by C. *rodentium* (Φ*stx*$_{2dact}$) promotes colonization of the colonic mucosa.
A. Faecal shedding by mice infected with the designated strain, represented as the mean cfu (± SEM) of groups of five mice. (*$P < 0.05$; **$P < 0.01$; and ***$P < 0.001$; by repeated measures two-way ANOVA followed by Bonferroni post-tests.) Data represent one of five experiments.
B. Faecal shedding by mice infected with *C. rodentium* (Φ*stx*$_{2dact}$)Δ*tir*/pTir$_{WT}$ and *C. rodentium* (Φ*stx*$_{2dact}$)Δ*tir*/pTir$_{Y471F}$ at 6 days post-infection (left panel). Luminal colonization was measured by determining cfu ml^{-1} of luminal washings (second panel). Intestinal colonization (caecum and colonic) was measured by determining cfu mg^{-1} of tissue homogenate at 6 days post-infection (right two panels). Data represent a compilation of eight experiments, with three-to-ten mice per group. Each data point represents one mouse. Horizontal line indicates the mean. Fold increase represents the fold change between colonization by *C. rodentium* (Φ*stx*$_{2dact}$)Δ*tir*/pTir$_{WT}$ and *C. rodentium* (Φ*stx*$_{2dact}$)Δ*tir*/pTir$_{Y471F}$. Error bars indicate ± SEM. (**$P < 0.01$ and ***$P < 0.001$.)
C. Caecal and colonic sections of mice infected with *C. rodentium* (Φ*stx*$_{2dact}$)Δ*tir*/pTir$_{WT}$ or *C. rodentium* (Φ*stx*$_{2dact}$)Δ*tir*/pTir$_{Y471F}$ were taken at 10 days post-infection and stained with DAPI (blue) and anti-*Citrobacter* antibody (green). Faecal shedding by each strain was equivalent at both time points. Mice infected with *C. rodentium* (Φ*stx*$_{2dact}$)Δ*tir*/pTir$_{WT}$ and *C. rodentium* (Φ*stx*$_{2dact}$)Δ*tir*/pTir$_{Y471F}$ had faecal bacterial loads of 4.8×10^7 g^{-1} and 3.6×10^7 g^{-1} respectively. Magnification of IF images is 600×. White arrows indicate bacteria.

shedding, particularly late in infection (Fig. 5A). Pooled results of independent experiments revealed that infection with *C. rodentium* (Φ*stx*$_{2dact}$)Δ*tir*/pTir$_{Y471F}$ resulted in a five-fold decrease in peak faecal shedding compared with the isogenic *C. rodentium* (Φ*stx*$_{2dact}$)Δ*tir*/pTir$_{WT}$ (Table 1). [Peak faecal shedding of *C. rodentium* (Φ*stx*$_{2dact}$)Δ*tir*/pTir$_{WT}$ and *C. rodentium* (Φ*stx*$_{2dact}$)Δ*tir*/pTir$_{Y471F}$ was approximately six- and approximately fourfold higher than their non-lysogenic counterparts, respectively, consistent with the observation that lysogeny of non-toxigenic *C. rodentium* by Φ*stx*$_{2dact}$ promotes colonization; Table 1.] As above, the decreased faecal shedding by *C. rodentium* (Φ*stx*$_{2dact}$)Δ*tir* harbouring pTir$_{Y471F}$ was not a function of plasmid loss, because pTir$_{WT}$ and pTir$_{Y471F}$ were equivalently stable throughout murine infection (Table S4). Thus, a moderate decrease in faecal shedding was observed in a pedestal-defective strain, regardless of the presence or absence of Φ*stx*$_{2dact}$ (see Fig. 4A–C).

To determine whether *C. rodentium* (Φstx$_{2dact}$)Δ*tir*/pTir$_{Y471F}$, displayed a more pronounced defect in colonization of the colon than of the caecum, as was the case for the non-lysogenic *C. rodentium*Δ*tir*/pTir$_{Y471F}$, we quantified viable bacteria stably associated with each of these intestinal segments at a time point close to peak colonization. At 6 days post-infection, faecal shedding was approximately fourfold higher in mice infected with the pedestal-competent *C. rodentium* (Φstx$_{2dact}$) derivative than in mice infected with the isogenic pedestal-defective strain (Fig. 5B, first panel). The difference did not reach statistical significance, but was similar to the difference observed at 6 days post-infection in the kinetic analysis of the same strains (Fig. 5A), and to results observed for non-lysogenic *C. rodentium* derivatives (Fig. 4C, first panel). Likewise, a relatively small (approximately three-fold and statistically insignificant) difference in the concentration of the two strains in luminal washings was observed (Fig. 5B, second panel). Caecal colonization in mice infected with the pedestal-competent *C. rodentium* (Φ*stx*$_{2dact}$) was approximately sixfold higher than in mice infected with the pedestal-defective strain (Fig. 5B, third panel), a difference nearly identical to that observed for the non-lysogenic *C. rodentium* derivatives (Fig. 4C, third panel), but one that, in contrast, reached statistical significance ($P < 0.01$). Notably, colonic colonization of mice

infected with the pedestal-competent strain was more than 11-fold ($P < 0.001$) higher than in mice infected with the pedestal-defective strain (Fig. 5B, fourth panel). Thus, the ability to generate actin pedestals was associated with: (i) a relatively small increase in the number of bacteria present in the stool or luminal washings, (ii) a modest but significant increase in colonization of the caecum, and (iii) a striking and significant increase in colonization of the colon.

To assess the association of pedestal-competent and pedestal-defective *C. rodentium* (Φ*stx*$_{2dact}$) with the mucosal surface during infection, we visualized infected intestinal segments by IF microscopy. At a time point near peak faecal shedding when faecal shedding of the two strains was similar, we found that the pedestal-competent *C. rodentium* (Φ*stx*$_{2dact}$) adhered to the mucosal surfaces of both the caecum and the colon (Fig. 5C, top panels). Caecal and colonic samples of approximately 72% of mice (13/18) infected with this strain scored positive by microscopic assessment of mucosally associated *C. rodentium*, (Table 2). Bacteria closely adhered to the mucosal surface and penetrated deep into the crypts (Fig. 5C). In contrast, only 26% of caecal specimens (5/19) from mice infected with pedestal-defective *C. rodentium* scored positive, a rate approximately threefold lower than for mice infected with pedestal-competent bacteria ($P < 0.005$, Table 2; Fig. 5C). Furthermore, similar to our observation for non-toxigenic pedestal-defective *C. rodentium*, none of the 19 colonic mucosal samples scored positive, a highly significant ($P < 0.0001$) difference compared with samples from mice infected with pedestal-competent *C. rodentium* (Φ*stx*$_{2dact}$). These results are also consistent with the striking (~ 11-fold) colonic colonization decrease seen with pedestal-defective *C. rodentium,* as assessed by viable counts (Fig. 5B). Importantly, the defect in colonization of the colonic mucosa by pedestal-defective *C. rodentium* (Φ*stx*$_{2dact}$) was significantly ($P < 0.02$) greater than the defect in colonization of the caecal mucosa by this strain. Thus, pedestal-defective bacteria are significantly more impaired in colonic than in caecal colonization.

To examine more closely the interaction of pedestal-competent and pedestal-defective derivatives of *C. rodentium* (Φ*stx*$_{2dact}$) with the mucosa, infected caecal and colonic tissues were evaluated by TEM. As expected, AE lesions appeared on the caecal and colonic mucosa of mice infected with *C. rodentium* (Φ*stx*$_{2dact}$)Δ*tir*/pTir$_{WT}$ (data not shown). *C. rodentium* (Φ*stx*$_{2dact}$)Δ*tir*/pTir$_{Y471F}$ was closely associated with the mucosal surface of the caecum, although typical AE lesions were not seen (data not shown). Consistent with our IF microscopy results, following infection with *C. rodentium* (Φ*stx*$_{2dact}$)Δ*tir*/pTir$_{Y471F}$, TEM revealed virtually no associated bacteria (data not shown). Thus, the ability to generate actin pedestals appears to be more critical to epithelial colonization of the colon than of the caecum.

C. rodentium *(Φ*stx$_{2dact}$*) producing TirY471F is severely diminished in the ability to cause Stx-mediated systemic disease*

The ability of pedestal-competent bacteria to colonize the colonic mucosa might be predicted to promote Stx-mediated local and systemic disease. We evaluated intestinal and renal pathology in mice infected with *C. rodentium* (Φ*stx*$_{2dact}$)Δ*tir*, *C. rodentium* (Φ*stx*$_{2dact}$)Δ*tir*/pTir$_{WT}$, or *C. rodentium* (Φ*stx*$_{2dact}$)Δ*tir*/pTir$_{Y471F}$. As previously observed, mice infected with *C. rodentium* (Φ*stx*$_{2dact}$)Δ*tir* displayed no intestinal damage (Fig. 6, left column, arrows; Mallick *et al.*, 2012b). In contrast, infection by *C. rodentium* (Φ*stx*$_{2dact}$)Δ*tir*/pTir$_{WT}$ resulted in destruction of the intestinal mucosa, colitis, acute ischemic injury, and inflammation at 10 days post-infection (Fig. 6, middle column, arrowheads). Areas of necrosis and degenerative changes in the epithelial cells with crypt withering were also observed (Fig. 6, middle column, asterisks). As expected, the impaired ability of *C. rodentium* (Φ*stx*$_{2dact}$)Δ*tir*/pTir$_{Y471F}$ to colonize the colonic mucosa was associated with the lack of colonic damage (Fig. 6, right column).

The Stx receptor Gb_3 is highly enriched in mouse renal tubules (Psotka *et al.*, 2009). Confirming a previous report (Mallick *et al.*, 2012b), *C. rodentium* (Φ*stx*$_{2dact}$)Δ*tir*/pTir$_{WT}$ infection resulted in damage to the proximal tubules, reflected by flattening flattened of the epithelial lining, the presence of pyknotic nuclear material, and sloughing of dead cells in the tubular lumen (Fig. 7A, middle panel, arrowheads). Mitotic activity, indicative of regeneration and repopulation of the proximal tubules, was also observed in some mice (data not shown). These pathological changes were associated with significant proteinuria (Fig. 7B). In contrast, no renal damage or proteinuria was observed upon infection with *C. rodentium* (Φ*stx*$_{2dact}$)Δ*tir*/pTir$_{Y471F}$ (Fig. 7A, right panel; 7B).

Consistent with previous findings in our infection model and other murine models of Stx intoxication (Keepers *et al.*, 2006; Sauter *et al.*, 2008; Mohawk and O'Brien, 2011), *C. rodentium* (Φ*stx*$_{2dact}$) but not *C. rodentium* (Φ*stx*$_{2dact}$)Δ*tir*, induced weight loss and death (Mallick *et al.*, 2012b; data not shown). pTir$_{WT}$ complemented *C. rodentium* (Φ*stx*$_{2dact}$)Δ*tir* for these defects, but as previously observed (Mallick *et al.*, 2012b), complementation appeared to be incomplete: compared to mice infected with *C. rodentium* (Φ*stx*$_{2dact}$), mice infected with *C. rodentium* (Φ*stx*$_{2dact}$)Δ*tir*/pTir$_{WT}$ displayed an ~ 3- to 7-day delay in the kinetics of weight loss and death compared with those infected with *C. rodentium* (Φ*stx*$_{2dact}$) [Fig. 7C and D; compared to Fig. 6 in reference (Mallick *et al.*,

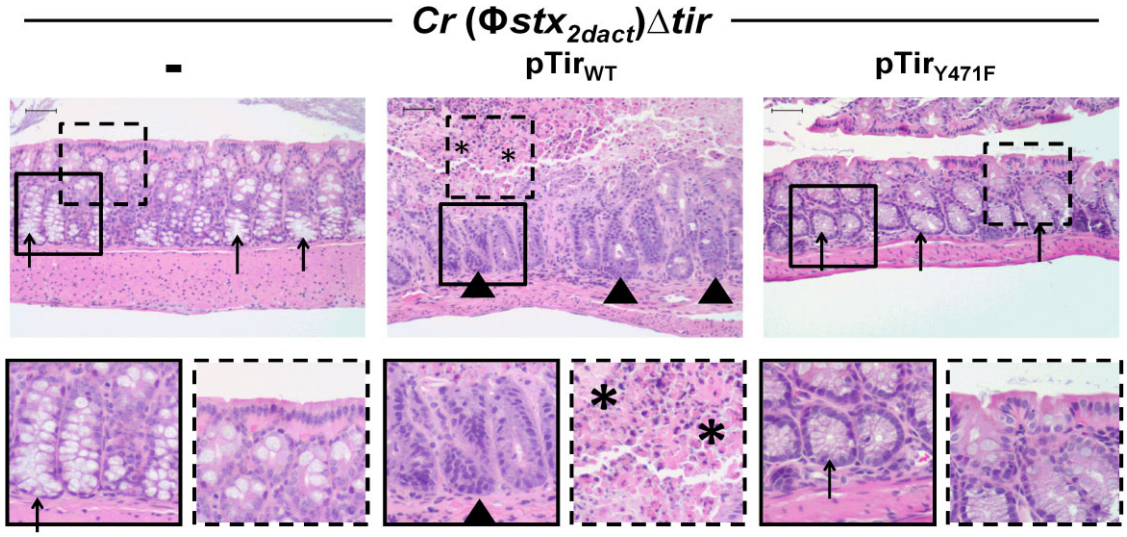

Fig. 6. Tir-mediated actin assembly by *C. rodentium* (Φ*stx*$_{2dact}$) promotes intestinal damage. H&E-stained intestinal sections of mice infected with the designated strain, taken at 10 days post-infection, are shown at 200× magnification (top row). Bottom row shows a higher magnification of the designated square in the image above. Arrowheads indicate areas of inflammation, arrows indicate areas of goblet cells, and asterisks indicate areas of mucosal surface destruction and necrosis. Scale is 50 μm.

2012b)], and a survival rate of 37.5% versus 0% (Table 3; Mallick *et al.*, 2012b; $P < 0.05$).

A rigorous logistic analysis of relative risk factors for lethal infection utilizing the relatively large number (i.e. 40) of mice infected with *C. rodentium* (Φ*stx*$_{2dact}$)Δ*tir*/pTir$_{WT}$ revealed two critical parameters. First, the survival rate after stratification for peak faecal load revealed that a one-log increase in faecal colonization corresponded to a 5.4-fold (95% CI of 1.5- to 19.2-fold) increased risk of death [Table 3, '*C. rodentium* (Φ*stx*$_{2dact}$)Δ*tir*/pTir$_{WT}$'], indicating that, not surprisingly, for a given Stx-producing strain, faecal load correlates with lethality. Second, and more notably, the ability to form actin pedestals was highly associated with lethality, even after accounting for peak faecal counts. Among mice with peak faecal loads of 7.7 to 8.3 Log cfu g^{-1} faeces, *C. rodentium* (Φ*stx*$_{2dact}$)Δ*tir*/pTir$_{WT}$ infection was associated with a mortality rate of 60% (3/5), as opposed to no mortality (0/8) resulting from *C. rodentium* (Φ*stx*$_{2dact}$)Δ*tir*/pTir$_{Y471F}$ infection (0/8; $P < 0.05$; Table 3). Similarly, for mice with peak faecal loads of 8.3 to 9.1 Log cfu g^{-1} faeces, *C. rodentium* (Φ*stx*$_{2dact}$)Δ*tir*/pTir$_{WT}$ infection resulted in a mortality rate of 53% (8/15), compared to 0% (0/5) for mice infected with *C. rodentium* (Φ*stx*$_{2dact}$)Δ*tir*/pTir$_{Y471F}$ ($P < 0.05$; Table 3). Consistent with the stratification analysis, a logistic regression analysis showed that even when the levels of faecal shedding were normalized, mice infected with *C. rodentium* (Φ*stx*$_{2dact}$)Δ*tir*/pTir$_{WT}$ were 16-fold (95% CI of 1.7- to 147.4-fold) more likely to succumb to lethal infection than were mice infected with the pedestal-defective *C. rodentium* (Φ*stx*$_{2dact}$)Δ*tir*/pTir$_{Y471F}$ strain. Thus, Tir-mediated actin pedestal formation not only promotes colonization of the colonic mucosa, but greatly facilitates Stx-mediated lethal systemic disease, even when considered independently from levels of faecal shedding.

Discussion

Tir is required for efficient cell attachment (Nougayrede *et al.*, 2003) and for intestinal colonization by AE pathogens (Schauer and Falkow, 1993b; Tzipori *et al.*, 1995; Marches *et al.*, 2000; Deng *et al.*, 2003; Ritchie *et al.*, 2003). Tir also promotes the formation of actin pedestals, but the role of pedestals in colonization and disease has been unclear (Deng *et al.*, 2003; Vlisidou *et al.*, 2006; Schuller *et al.*, 2007b). For example, an EHEC mutant lacking the type III-secreted effector EspF$_U$ (also known as TccP; Garmendia *et al.*, 2004) which, like a strain expressing TirY471F or TirY471A, was capable of Tir-mediated cell attachment but defective for pedestal formation on cultured cells, showed no discernible defect in colonization of calves or lambs (Vlisidou *et al.*, 2006). On the other hand, an equivalent mutant displayed a mild (approximately two- to sixfold, depending on the intestinal site) colonization defect in infant rabbits, and formed bacterial aggregates on the intestinal wall of infant piglets that were smaller than wild type (Ritchie *et al.*, 2008). In a systematic analysis of the role of pedestal formation during infection, Crepin and co-workers found that *C. rodentium* producing TirY471A from a chromosomal locus formed AE lesions on colonic mucosa and was present in faeces at wild type levels (Crepin *et al.*, 2010). However,

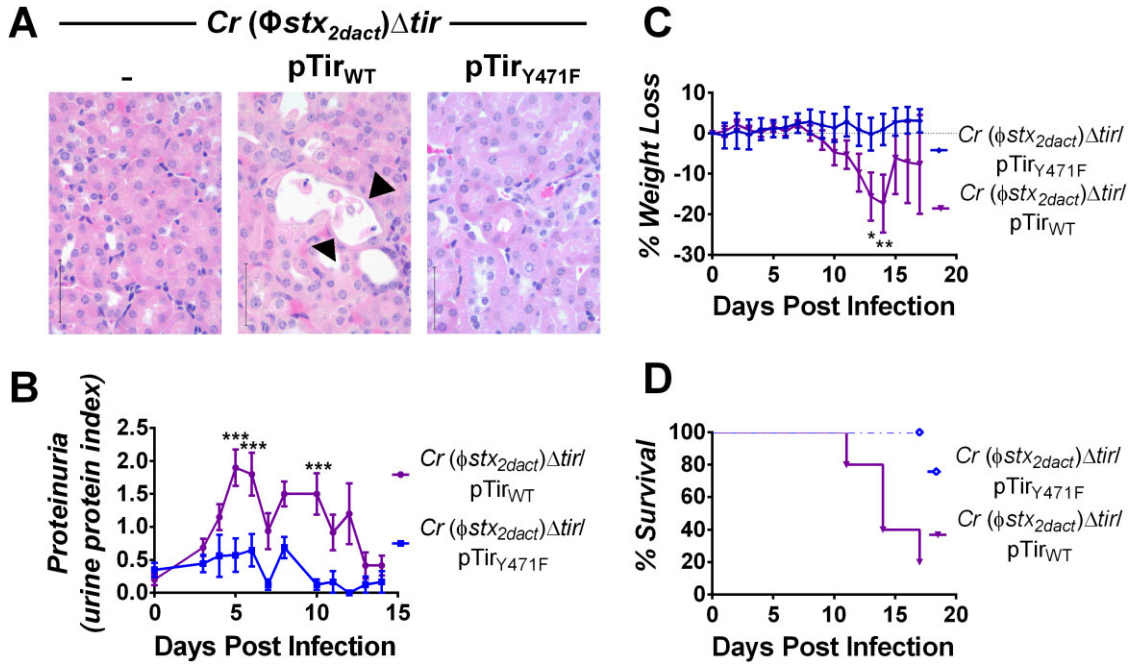

Fig. 7. Tir-mediated actin assembly by *C. rodentium* (Φ*stx*$_{2dact}$) promotes renal damage, weight loss, and death.
A. H&E-stained kidney sections from mice infected with the designated strain, taken at 10 days post-infection. Sloughing and attenuation of epithelial cells within the proximal tubules is indicated by arrowheads. Scale bars are 50 μm, magnification, 600×.
B. Urine protein content in mice infected with the designated strain is represented as mean proteinuria index (± SEM), where 0 indicates undetectable protein, 0.5 indicates trace amounts, 1.0 = ~ 30 mg dl^{-1}, 2.0 = ~ 100 mg dl^{-1}, and 3.0 = ~ 500 mg dl^{-1}. Data represent one of two experiments, with 5–10 mice per group. (***$P < 0.001$ by repeated measures two-way ANOVA followed by Bonferroni post-tests.) 6/10 mice infected with *C. rodentium* (Φ*stx*$_{2dact}$)Δ*tir*/pTir$_{WT}$ developed proteinuria during infection and fully recovered by 2 weeks post-infection; in addition, as described in *Experimental procedures*, the return of average proteinuria towards baseline depicted in the graph preceded clinical recovery of individual mice by a few days, as described in *Experimental procedures*.
C. Weight loss in mice infected with the designated strain was determined and expressed as percent change from day 0 to 8. Shown are the means (± SEM) of five mice per group. Data represent one of six independent experiments. (*$P < 0.05$ and **$P < 0.01$ by repeated measures two-way ANOVA followed by Bonferroni post-tests; in addition, as described in *Experimental procedures*, the return of average weight towards baseline depicted in the graph preceded clinical recovery of individual mice by a few days.)
D. Percent survival of mock-infected mice or mice infected with the designated strain. Data shown represent one of five experiments. Statistical significance was determined using a Log-rank (Mantel-Cox) test and revealed a significant ($P < 0.05$) difference between the two groups.

in co-infection experiments, mutant bacteria were significantly outcompeted by wild type bacteria at late time points, suggesting a colonization defect for the pedestal-incompetent mutant.

In the current study, we first investigated the role of Tir-mediated actin assembly in colonization of a mouse specifically defective for N-WASP production in the intestine. iNWKO mice were viable, fertile, displayed normal

Table 3. Actin pedestal formation promotes lethal infection.

	Cr (Φ*stx*$_{2dact}$)Δ*tir*/pTir$_{WT}$		*Cr* (Φ*stx*$_{2dact}$)Δ*tir*/pTir$_{Y471F}$	
Range of faecal shedding (log)	Average log faecal shedding	% Lethality (# dead/total)	Average log faecal shedding	% Lethality (# dead/total)
9.7–10.7	9.8	80% (4/5)	na	na
9.1–9.7	9.3	91% (10/11)	9.4	100% (1/1)
8.3–9.1	8.8	53% (8/15)	8.8	0%[a] (0/5)
7.7–8.3	8.0	60% (3/5)	8.0	0%[a] (0/8)
Below 7.7	4.8	0% (0/4)	7.4	0% (0/6)
Total	8.8	62.5% (25/40)	8.1	5% (1/20)

a. Statistically significant defect in lethality compared to mice infected with *C. rodentium* (Φ*stx*$_{2dact}$)Δ*tir*/pTir$_{WT}$ ($P < 0.05$).
na, not applicable.

crypt-villous architecture, and exhibited no inflammatory changes. These mice were incapable of supporting mucosal colonization upon infection by *C. rodentium*, and neither *C. rodentium* nor *C. rodentium* (Φstx_{2dact}) reached the levels of faecal bacteria found in N-WASP-proficient littermate controls. On the other hand, iNWKO mice displayed wild type sensitivity to *S. enterica* infection.

Similarly, when pedestal formation was blocked by the TirY471F bacterial mutation rather than by the iNWKO mouse mutation, faecal shedding of *C. rodentium* or *C. rodentium* (Φstx_{2dact}) by wild type mice was reduced. (The shedding level, although reduced, was still considerably more than that observed for iNWKO mice, a finding that may indicate an additional role for N-WASP in *C. rodentium* colonization beyond pedestal formation.) The diminished faecal shedding of the pedestal-incompetent *C. rodentium tir* mutant was highly statistically significant, in contrast to the near wild type levels of faecal shedding by a strain producing TirY474A reported by Crepin and co-workers and mentioned above (Crepin *et al*., 2010). These investigators compared the function of a single-copy wild type or mutant *tir* alleles inserted into the endogenous chromosomal *tir* locus. In contrast, we transformed Tir-deficient strains with a Tir-encoding plasmid, which resulted in only partial complementation. Expression of *tir* from a multicopy plasmid such as that used here may result in non-wild type levels of Tir per cell, and the efficiency of Tir translocation via the type III secretion system may be influenced by the level of Tir produced. Notably, Deng and co-workers found that infection of mice with a *C. rodentium* strain producing plasmid-encoded, pedestal-incompetent TirY471F resulted in lower than wild type bacterial titres in stool-filled colonic samples, although the 4.5-fold difference did not reach statistical significance (Deng *et al*., 2003). Although these investigators presented TEM evidence of AE lesions beneath bound, TirY471F-producing bacteria, a systematic IF microscopic analysis to measure the relative frequency of mucosa-associated bacteria, such as was performed in this study, was not undertaken. Regardless of the aetiology of different conclusions among studies addressing the role of AE pathogen-induced pedestal formation during infection, our particular experimental system appears to be very sensitive to differences in Tir function, one that revealed a highly significant ($P < 0.001$) colonization defect of the TirY471F mutant.

Upon quantification of bacteria associated with stool, luminal washings, caecum, or colon, production of TirY471F was associated with the most striking colonization defect in the colon [~ 16- and 11-fold for *C. rodentium* and *C. rodentium* (Φstx_{2dact}) respectively] than in the caecum (approximately sixfold for both strains; Figs 4 and 5, Table 2). Quantitative analysis of epithelial colonization by *C. rodentium* (Φstx_{2dact}) in the intestine, visualized by IF microscopy, revealed that the pedestal-defective mutant was associated with a significantly more severe mucosal attachment defect in the colon than in the caecum. The underlying basis for the colon-specific colonization activity of pedestal formation is not clear. The caecum is the initial colonization site for *C. rodentium* in mice (Wiles *et al*., 2004) and for EHEC in lambs, calves, and chickens (Beery *et al*., 1985; Dean-Nystrom *et al*., 1999; Wales *et al*., 2001; Wiles *et al*., 2004), indicating that this intestinal segment, which is a blind pouch with minimal bulk flow, may provide AE pathogens with an anatomically hospitable environment in which to establish infection (Sherman and Boedeker, 1987). We postulate that in this niche, pedestal formation is less critical for successful mucosal colonization.

The ability of a pedestal-defective AE pathogen to colonize the caecum might be predicted to mute any decrease in faecal shedding due to a defect in colonization of other intestinal segments. In fact, we found that the 11- to 16-fold defect in colonic colonization was associated with only an approximately fourfold defect in faecal shedding, possibly due to luminal bacteria released from the (efficiently colonized) caecum. Given that many studies utilize faecal shedding as a convenient serial readout of intestinal colonization (Mundy *et al*., 2004; Marches *et al*., 2005; Ritchie and Waldor, 2005; Vlisidou *et al*., 2006; Girard *et al*., 2009; Crepin *et al*., 2010), our finding that pedestal formation may play an essential role in mucosal colonization for only a subset of intestinal segments could partially explain varying apparent defects in colonization by pedestal-defective mutants in other studies.

Pedestal formation might promote colonic colonization by any of several mechanisms. First, by promoting (indirect) attachment of the bacterium to the host cytoskeleton, pedestal formation may stabilize bacterial binding at the cell surface. Indeed, whereas we found that *C. rodentium* (Φstx_{2dact}) expressing TirY471F bound to cultured murine cells indistinguishably from *C. rodentium* (Φstx_{2dact}) producing wild type Tir, the ability of EHEC to promote actin assembly is associated with enhanced binding to cultured mammalian cells (S. Battle and G. Hecht, pers. comm.). This putative stable attachment, in addition to facilitating intestinal retention of *C. rodentium* in the face of luminal bulk flow, may allow the pathogen to occupy an environmental niche protected from intense nutritional competition with commensal bacteria located in the lumen (Kamada *et al*., 2012). Second, N-WASP has been previously shown to promote type III secretion by EHEC and (to a lesser degree) EPEC (Vingadassalom *et al*., 2010). In addition, a mutation in EHEC Tir that diminishes actin pedestal formation is associated with a moderate (but significant) defect in type III translocation (S. Battle and G. Hecht, pers. comm.). These findings raise the possibility that, given the requirement of effector translocation for

efficient colonization (Deng *et al*., 2004; Ritchie and Waldor, 2005), the defect in *C. rodentium* colonization observed in the iNWKO mice may in part be due to diminished type III translocation. Finally, the dynamic nature of actin turnover and assembly in pedestals promotes the movement of EHEC or EPEC on the surface of cultured mammalian cells (Sanger *et al*., 1996; Shaner *et al*., 2005), and similar to actin-based cell-to-cell spread of *Vaccinia* virus (Goldberg, 2001), pedestal formation may promote the spread of the pathogen, consistent with the smaller than wild type aggregates of pedestal-defective EHEC on the mucosal surface (Ritchie *et al*., 2008).

The enhanced mucosal colonization facilitated by actin pedestal formation was associated with dramatically greater Stx-mediated pathogenicity. First, iNWKO mice exhibited less intestinal and renal damage, maintained body weight, and uniformly survived infection by *C. rodentium* (Φ*stx*$_{2dact}$), in contrast to N-WASP-proficient littermate controls, who lost weight and suffered a 35% lethality rate. Second, mice infected with pedestal-defective *C. rodentium* (Φ*stx*$_{2dact}$) demonstrated less intestinal damage and no renal dysfunction or weight loss. The dramatically enhanced Stx-mediated disease induced by pedestal-competent *C. rodentium* (Φ*stx*$_{2dact}$) was not simply a function of bacterial load in the lumen, because pedestal-competent *C. rodentium* (Φ*stx*$_{2dact}$) was associated with a 16-fold greater risk of death compared to pedestal-defective bacteria after normalizing for the peak faecal load of bacteria.

Although we cannot rule out the possibility that bacteria bound to the mucosal surface produce more Stx than luminal bacteria, it is also possible that pedestal formation directly or indirectly facilitates Stx penetration of the epithelial barrier, leading to systemic intoxication (Nakao and Takeda, 2000). For example, type III effectors such as EspF disrupt the epithelial barrier (McNamara *et al*., 2001; Guttman *et al*., 2006; Holmes *et al*., 2010), and as mentioned above, pedestal formation promotes not only EHEC attachment but also the efficiency of effector translocation per bound EHEC (S. Battle and G. Hecht, pers. comm.). In addition, pedestal formation, by disrupting the apical actin network, may itself compromise tight junctions, as several tight junction components are aberrantly localized to pedestals on cultured cells (Hanajima-Ozawa *et al*., 2007; Peralta-Ramirez *et al*., 2008). Finally, the proximity of Stx production at the mucosal surface, perhaps in combination with the intestinal damage observed in this infection (Mallick *et al*., 2012b), may promote toxaemia. Interestingly, infection by the recently emerged *E. coli* O104:H4, a Stx-producing strain that is related to enteroaggregative *E. coli* (EAEC), is associated with a high rate of rapidly progressing Stx-mediated disease and HUS (Rasko *et al*., 2011). This strain is incapable of generating AE lesions, indicating that AE lesion formation is not an absolute requirement for Stx-mediated disease. Nevertheless, like EAEC, *E. coli* O104:H4 is highly adherent to cultured host cells (Beutin and Martin, 2012; Pierard *et al*., 2012), suggesting that Stx production in the context of tight bacterial adherence may promote severe Stx-mediated disease (Bielaszewska *et al*., 2011). Thus, future investigation into the relationship between mucosal colonization promoted by actin pedestal formation and systemic disease promoted by Stx may provide general insights into the pathogenesis of toxigenic mucosal pathogens.

Experimental procedures

Phage and bacterial strains

Bacterial and phage strains used in this study are listed in Table S1. The phage used to generate *C. rodentium* (Φ*stx*$_{2dact}$) was Φ1720a-02 Δ*Rz*::*cat* (Table S1), derived from STEC strain EC1720 (Gobius *et al*., 2003). EC1720 was originally thought to be lysogenized by a single Stx-producing phage, Φ1720a (Gobius *et al*., 2003), also termed Φ1720a-01 (Mallick *et al*., 2012b). We subsequently showed that EC1720 was also lysogenized by a second Stx-producing phage, Φ1720a-02, this one producing Stx2dact (Mallick *et al*., 2012b). A chloramphenicol resistance cassette was then inserted into the *Rz* locus of Φ1720a-02 to generate the Stx2dact-producing phage Φ1720a-02 Δ*Rz*::*cat* (Mallick *et al*., 2012b). This latter phage was originally termed 'λ*stx*$_{2dact}$' (Mallick *et al*., 2012b). However, subsequent DNA sequencing and annotation of Φ1720a-02 Δ*Rz*::*cat* Δ*stx*$_{2dact}$::*kan*, a derivative of Φ1720a-02 Δ*Rz*::*cat* harbouring a kanamycin resistance cassette in *stx*$_{2dact}$, revealed that Φ1720a-02 (GenBank Accession No. KF03044) is only distantly related to phage λ (M. Osburne and A. Tai, pers. comm.). Therefore, we have removed 'λ' from all designations of this phage and now denote it as '*Φstx*$_{2dact}$'.

Bacterial growth conditions

Bacterial strains were cultured in Luria–Bertani broth (LB) (Miller) at 37°C, unless indicated otherwise. Antibiotics were used at the following concentrations: kanamycin, 25 μg ml^{-1}; zeocin, 75 μg ml^{-1}; chloramphenicol, 10 μg ml^{-1}; tetracycline, 5 μg ml^{-1}; and streptomycin, 20 μg ml^{-1}.

Plasmid isolation, primers, and sequencing

Plasmids used this study are listed in Table S2. Plasmid DNA was isolated using the QIAprep Spin Miniprep Kit (QIAgen, Valencia, CA). Primers were purchased from Invitrogen (Grand Island, NY) and are listed in Table S3. Sequencing was performed at Tufts University Core Sequencing Facility (Boston, MA).

Construction of a C. rodentium *TirY471F plasmid*

pEM340 'pTir$_{Y471F}$' was constructed using SLIM as previously described (Chiu *et al*., 2004), using the following primers: R-Oli178, F-Oli179, R-Oli180, and F-Oli181 (Table S3). Plasmid

constructs were confirmed by sequencing and pedestal formation was tested by phalloidin and DAPI staining of infected monolayers as previously described (Mallick *et al*., 2012a).

Infection and binding analysis of C. rodentium *(Φstx$_{2dact}$) and mutants on cultured cells*

Filamentous actin staining (FAS) assay and bacterial binding quantification was done as previously described (Mallick *et al*., 2012a).

Generation, characterization, and infection of conditional, intestinal, N-WASP$^{-/-}$ mice

The PCR strategy for developing and genotyping the iNWKO mouse has been previously described (Cotta-de-Almeida *et al*., 2007; Lyubimova *et al*., 2010). iNWKO breeder mice and offspring were housed at the UMass Medical School (UMMS) animal facility, the Center for Comparative Medicine at the Massachusetts General Hospital, and/or the Boston Children's Hospital animal facility. iNWKO mice were generated by breeding female conditionally targeted *N-Wasp$^{flox/flox}$* mice, in which exon 2 of N-WASP is flanked by LoxP sites (Cotta-de-Almeida *et al*., 2007; Lyubimova *et al*., 2010), with transgenic male *N-Wasp$^{flox/+}$*, tg$^{villin\text{-}Cre}$ mice expressing Cre recombinase under the intestine-specific promoter villin (el Marjou *et al*., 2004). This breeding resulted in approximately 15% of mice with the desired genotype (*N-wasp$^{flox/flox}$, tg$^{villin\text{-}Cre}$*). Genotyping was performed by Transnetyx (Cordovia, TN). Throughout the text, littermate control mice are defined as those mice in the same litter as the iNWKO mice with any of the following genotypes: *N-Wasp$^{+/+}$*, N-Wasp$^{flox/+}$, N-Wasp$^{flox/flox}$, or *N-Wasp$^{flox/+}$*, tg$^{villin\text{-}Cre}$.

For Western blotting, intestinal epithelial cells (IECs) were isolated from 8-week-old littermate control or iNWKO mice by EDTA dissociation, as previously described (Whitehead and Robinson, 2009), and lysed with ice-cold RIPA buffer (Tris 50 mM, NaCl 150 mM, SDS 0.1%, sodium deoxycholate 0.5%, NP-40 1%, complete protease inhibitor cocktail). IEC protein extracts were separated by SDS gel electrophoresis, and transferred onto nitrocellulose membrane as previously described (Campellone *et al*., 2008). Immunoblotting was performed with rabbit polyclonal anti-N-WASP (1:2000) (kindly provided by Dr Marc Kirshner), followed by HRP-conjugated goat anti-rabbit secondary antibody (1:3000) (Cell Signaling, Danvers, MA), and visualized using enhanced chemiluminescence (ECL) (GE Healthcare Life Sciences, Piscataway, NJ).

All infection experiments using iNWKO mice were approved by UMMS Department of Animal Medicine and the UMMS IACUC (protocol-2049 to JML and A-1993-11 to BAM), the Subcommittee on Research Animal Care of the Massachusetts General Hospital (protocol-2005N000266), and the Children's Hospital Animal Care and Use Committee (protocol-11-04-1918). The murine infection experiments included age and sex matched littermate controls. Inoculum doses for infection of iNWKO mice and littermate controls were $\sim 5 \times 10^8$ cfu and $\sim 1 \times 10^9$ cfu for GFP-*C. rodentium* and *C. rodentium* (*Φstx$_{2dact}$*) respectively. Faecal shedding, per cent body weight loss, and proteinuria indices were determined as previously described (Mallick *et al*., 2012b). Maximal faecal shedding was defined as the highest titre of bacteria in the stool at any time point throughout the course of infection. Maximal percent body weight loss was defined as the maximum amount lost at any time point throughout the course of experiment. Note that mice that had suffered weight loss and proteinuria but survived infection ultimately cleared intestinal bacteria, regained weight to original baseline, and recovered from proteinuria. However, the rate of clinical recovery of individual mice was somewhat slower than that which might be inferred from graphs of average post-infection weight loss and proteinuria (Figs 3E and 7B and C), because mice with the most severe weight loss and proteinuria were euthanized, thus enriching the set of surviving mice for those that were less affected by infection. Hence, the depicted average post-infection weight and proteinuria, which reflects this set of surviving mice, returned towards baseline more quickly than the weight and proteinuria of individual mice.

For IF, sections from the proximal and distal colon were embedded in OCT and 5 μm frozen sections were electrostatically adhered to glass slides. Upon reaching room temperature, slides were fixed in 4% paraformaldehyde for 10 min, stained with phalloidin, and mounted with Vectashield mounting medium with DAPI (Vector Laboratories, Burlingame, CA). Histological and IF identification of GFP+ bacteria was performed using an Olympus AX-70 upright fluorescence microscope (Olympus, Tokyo, Japan).

To quantify the intercrypt mucosal epithelium with adherent *C. rodentium*, intestinal sections from wild type and iNWKO mice were taken at 4 days post-infection with GFP-expressing *C. rodentium* (see Table S1). Sections were flash frozen in OCT and sectioned at 5 μm. Slides were fixed in 4% paraformaldehyde, stained with DAPI, and visualized with an upright epifluorescence microscope. Four sections from each tissue sample were examined, and the mucosal epithelium located between adjacent crypts (designated the intercrypt mucosal epithelium, ICME) was examined for the presence of adherent, GFP-positive bacteria. The mean percentage of ICME demonstrating intimately adherent bacteria per section was calculated. At least 30 ICME per section were examined.

To determine whether decreased colonization of iNWKO mice with wild type *C. rodentium* was due specifically to the absence of N-WASP rather than as a consequence of globally altered intestinal physiology (e.g. altered underlying immune reactivity or defective antimicrobial peptide secretion), littermate control and iNWKO mice were infected with 1.6×10^8 cfu *Salmonella* by oral gavage, as previously described (Srikanth *et al*., 2010). Bacterial recovery from tissue or stool in iNWKO compared to littermate control mice was quantified by viable counts. Tissues were processed for histology and evaluated as previously described (Mallick *et al*., 2012b).

Infection of wild type mice with engineered C. rodentium *strains expressing wild type or mutant Tir*

Wild type mice were purchased from Jackson Laboratories (Bar Harbor, ME) and housed in the UMMS animal facility. Eight-week-old, female, C57BL/6J mice were infected as previously described (Mallick *et al*., 2012b). All experimental groups contained at least five mice unless otherwise stated. The animal protocol (A-2049) was approved by the UMMS Department of Animal Medicine and the UMMS IACUC. Faecal shedding, weight loss, and proteinuria indices were determined as previously described (Mallick *et al*., 2012b).

Determination of peak faecal shedding of bacteria

The kinetics of faecal shedding occasionally differed from experiment to experiment even accounting for bacterial and murine strain, so for some comparisons we scored the peak of faecal shedding during the course of infection instead of shedding on a particular day after inoculation. In some instances, results from multiple experiments were pooled in order to increase the discrimination of statistically significant differences.

Determination of plasmid retention during murine infection

To assess the loss of Tir-producing plasmids during murine infection, groups of three mice were infected with *C. rodentium*Δ*tir*/pTir$_{WT}$, *C. rodentium*Δ*tir*/pTir$_{Y471F}$, *C. rodentium* (Φ*stx*$_{2dact}$)Δ*tir*/pTir$_{WT}$, or *C. rodentium* (Φ*stx*$_{2dact}$)Δ*tir*/pTir$_{Y471F}$. Faeces were collected on days 5, 7, 10 and 12 days post-infection. Faecal counts were determined by serial dilution and plating on MacLac (*C. rodentium*) or LB chloramphenicol [*C. rodentium* (Φ*stx*$_{2dact}$) strains] plates, and the per cent plasmid retention for each strain was determined by patching 100 colonies on to LB kanamycin plates. Plasmid retention was calculated by dividing the number of patched colonies that grew on kanamycin by the total number of colonies that grew on the MacLac or LB chloramphenicol plates, then multiplying by 100.

Analysis of tissue damage and bacterial association with mucosal surfaces by C. rodentium producing wild type or mutant Tir

Tissues were processed for histology and evaluated as previously described (Mallick *et al*., 2012b). For IF staining, at the indicated time post-infection, caecal or colonic sections were stained with DAPI to identify cell nuclei and anti-*Citrobacter* antibody [1:1600; a gift from David Schauer (Borenshtein *et al*., 2008)]. Samples were taken at 6 days post-infection for quantification of the IF samples (Table 2) and faecal counts at this time point were between 1.3×10^5 and 4.0×10^8 cfu per gram of stool for mice infected with the non-toxigenic *C. rodentium* strains and between 1.3×10^5 and 1.3×10^9 cfu per gram of stool for mice infected with the toxigenic *C. rodentium* (Φ*stx*$_{2dact}$) strains. To generate a score for epithelial colonization for each intestinal segment (Table 2), approximately 10 fields of caecal or colonic samples from each infected mouse were visualized microscopically for approximately 5 min and scored for bacteria adherent to the epithelium. The observation of one or more *C. rodentium* associated with the mucosal surface of a given segment resulted in a positive score for epithelial colonization of that segment. Data in Table 2 were compiled from three independent experiments using three-to-ten mice per group for each of the strains. Statistical significance was determined by a Student's *t*-test. TEM was performed as previously described (Mallick *et al*., 2012a,b).

Determination of cfu associated with different intestinal segments

At necropsy, the large intestine and faecal contents were removed. The large intestine was flushed with 1 ml PBS to remove loosely bound bacteria. Contents of the flush ('luminal washings') were collected and serial dilutions were plated on LB agar (± antibiotic). The intestine was divided into two parts: caecum and colon, homogenized, and serial dilutions were plated on LB agar (± antibiotic) to quantify the number of bacteria mg^{-1} of tissue.

Purification and generation of an anti-Citrobacter Tir antibody

Generation of an anti-*Citrobacter* Tir antibody was similar to the generation of an anti-EHEC Tir antibody, as previously described (Mallick *et al*., 2012a) with the exception that a *C. rodentium* Tir expression vector (pEM385 'pCrTirExp') was used. Primers F-190 and R-191 were used to amplify *C. rodentium tir* with NdeI and SalI flanking restriction sites (1.644 kb) from pEM129 'pTir$_{WT}$'. This PCR fragment was cloned into the NdeI and SalI sites of plasmid pET21b and transformed into *E. coli* DH5α. Transformants were selected on plates containing ampicillin. Candidate clones were verified by restriction digestion, PCR with primers R-iTirL and F-iTirU (480 bp), and sequencing. Upon sequence verification, pCrTirExp was transformed into BL21 DE3 and purified as previously described (Mallick *et al*., 2012a).

Tir immunoblotting

Citrobacter rodentium strains were cultured in DMEM + 0.1 M Hepes at 37°C, 5% CO_2 for 4.5 h. After centrifuging at 22 000 *g* for 10 min at room temperature, media was decanted and trichloroacetic acid was added in a 1:1 volume and incubated overnight at –20°C. The sample was then centrifuged at 22 000 *g* for 10 min at 4°C, the supernatant was decanted, and the pellet was resuspended in acetone and centrifuged at 20 800 *g* at 4°C for 10 min. Acetone was decanted and the pellet was air dried for 10 min and resuspended in water. Gel loading for SDS-PAGE was standardized to either final protein concentration quantified by Nanodrop (Thermo Fisher Scientific, Wilmington, DE) or final OD_{600}.

Stratification of colonization intervals

To compare the degree of lethality between mice infected with *C. rodentium* (Φ*stx*$_{2dact}$)Δ*tir*/pTir and *C. rodentium* (Φ*stx*$_{2dact}$)Δ*tir*/pTir$_{Y471F}$ at equivalent levels of faecal shedding, animals were grouped into five strata depending on peak faecal shedding levels (i.e. 9.7–10.7 Log cfu g^{-1}, 9.1–9.7 Log cfu g^{-1}, 8.3–9.1 Log cfu g^{-1}, 7.7–8.3 Log cfu g^{-1}, and below 7.7 cfu g^{-1}) (see Table 3). This grouping allowed for the maximum number of mice infected with each strain per grouping and the mean peak faecal colonization level within each grouping was nearly identical both in mice infected with *C. rodentium* (Φ*stx*$_{2dact}$)Δ*tir*/pTir and in mice infected with *C. rodentium* (Φ*stx*$_{2dact}$)Δ*tir*/pTir$_{Y471F}$. However, grouping of mice into two or three (rather than five) strata on the basis of peak faecal colonization also supported the conclusion that pedestal formation promotes lethality (S. Baker and E.M. Mallick, data not shown).

Statistical analysis

Differences in outcomes between strains were evaluated using Student's *t*-tests for two group comparisons, and one-way and two-factor repeated measures ANOVA appropriately for more

complex designs. In the presence of significant effects, pairwise comparisons were made using Tukey's HSD multiple comparisons procedure in the case of the one-way ANOVA, and Bonferroni adjusted Fisher's LSD tests in the case of the two-factor repeated measures ANOVA. Dichotomous categorical outcomes were modelled using logistic regression analysis using likelihood ratio chi-square tests to evaluate the significance of model terms. Differences in survival times were evaluated using Kaplan Meier Product Moment Survival Analysis with Log Rank tests to evaluate significance. Multivariate survival analysis was performed using Cox Proportionate Hazards models. The proportionate hazards assumption was tested by visual inspection of cumulative survival plots. Statistical significance was defined as effects with *P*-values less than or equal to 0.05. $^{*}P < 0.05$, $^{**}P < 0.01$, $^{***}P < 0.001$. Analyses were performed using GraphPad Prism and SPSS version 15.

Acknowledgements

We thank Z. Demma for invaluable assistance with *Salmonella* infection of mice. We thank the UMMS DERC for processing tissue for histology, L. Strittamatter and G. Hendricks of the UMMS EM Core for processing EM samples, L. Sonenshein and M. Osburne for thoughtful comments on the manuscript, Stephen Baker of UMMS for help with statistical analyses, Marc Kirshner for the N-WASP antibody, and the Tufts University CTSI consultative services. Electron microscopy on littermate control and iNWKO mice was performed in the Microscopy Core of the Center for Systems Biology/Program in Membrane Biology, which is partially supported by an Inflammatory Bowel Disease Grant DK43351 and a Boston Area Diabetes and Endocrinology Research Center (BADERC) Award DK57521. The work in this manuscript was supported by NIH Grants R21 AI092009 and R01 AI46454 to JML, NIH Grants P01 HL059561, R01 AI052354, 5P30DK034854 to SBS, NIH Grant K08 DK094966 to JJG, a Career Development Award from the Crohn's and Colitis Foundation of America to JJG, a Senior Research Award from the Crohn's and Colitis Foundation of America to JML and SBS, NIH Grants DK56754 and DK33506 to BAM, and by the National Center for Research Resources Grant No. UL1 RR025752 and the National Center for Advancing Translational Sciences, National Institutes of Health, Grant No. UL1 TR000073 to Tufts University CTSI consultative services.

References

Beery, J.T., Doyle, M.P., and Schoeni, J.L. (1985) Colonization of chicken cecae by *Escherichia coli* associated with hemorrhagic colitis. *Appl Environ Microbiol* **49:** 310–315.

Beutin, L., and Martin, A. (2012) Outbreak of Shiga toxin-producing *Escherichia coli* (STEC) O104:H4 infection in Germany causes a paradigm shift with regard to human pathogenicity of STEC strains. *J Food Prot* **75:** 408–418.

Bielaszewska, M., Mellmann, A., Zhang, W., Kock, R., Fruth, A., Bauwens, A., *et al*. (2011) Characterisation of the *Escherichia coli* strain associated with an outbreak of haemolytic uraemic syndrome in Germany, 2011: a microbiological study. *Lancet Infect Dis* **11:** 671–676.

Borenshtein, D., McBee, M.E., and Schauer, D.B. (2008) Utility of the *Citrobacter rodentium* infection model in laboratory mice. *Curr Opin Gastroenterol* **24:** 32–37.

Brady, M.J., Campellone, K.G., Ghildiyal, M., and Leong, J.M. (2007) Enterohaemorrhagic and enteropathogenic *Escherichia coli* Tir proteins trigger a common Nck-independent actin assembly pathway. *Cell Microbiol* **9:** 2242–2253.

Campellone, K.G. (2010) Cytoskeleton-modulating effectors of enteropathogenic and enterohaemorrhagic *Escherichia coli*: Tir, EspFu and actin pedestal assembly. *FEBS J* **277:** 2390–2402.

Campellone, K.G., and Leong, J.M. (2005) Nck-independent actin assembly is mediated by two phosphorylated tyrosines within enteropathogenic *Escherichia coli* Tir. *Mol Microbiol* **56:** 416–432.

Campellone, K.G., Giese, A., Tipper, D.J., and Leong, J.M. (2002) A tyrosine-phosphorylated 12-amino-acid sequence of enteropathogenic *Escherichia coli* Tir binds the host adaptor protein Nck and is required for Nck localization to actin pedestals. *Mol Microbiol* **43:** 1227–1241.

Campellone, K.G., Rankin, S., Pawson, T., Kirschner, M.W., Tipper, D.J., and Leong, J.M. (2004a) Clustering of Nck by a 12-residue Tir phosphopeptide is sufficient to trigger localized actin assembly. *J Cell Biol* **164:** 407–416.

Campellone, K.G., Robbins, D., and Leong, J.M. (2004b) $EspF_U$ is a translocated EHEC effector that interacts with Tir and N-WASP and promotes Nck-independent actin assembly. *Dev Cell* **7:** 217–228.

Campellone, K.G., Cheng, H.C., Robbins, D., Siripala, A.D., McGhie, E.J., Hayward, R.D., *et al*. (2008) Repetitive N-WASP-binding elements of the enterohemorrhagic *Escherichia coli* effector EspF(U) synergistically activate actin assembly. *PLoS Pathog* **4:** e1000191.

Caron, E., Crepin, V.F., Simpson, N., Knutton, S., Garmendia, J., and Frankel, G. (2006) Subversion of actin dynamics by EPEC and EHEC. *Curr Opin Microbiol* **9:** 40–45.

Chiu, J., March, P.E., Lee, R., and Tillett, D. (2004) Site-directed, Ligase-Independent Mutagenesis (SLIM): a single-tube methodology approaching 100% efficiency in 4 h. *Nucleic Acids Res* **32:** e174.

Cotta-de-Almeida, V., Westerberg, L., Maillard, M.H., Onaldi, D., Wachtel, H., Meelu, P., *et al*. (2007) Wiskott Aldrich syndrome protein (WASP) and N-WASP are critical for T cell development. *Proc Natl Acad Sci USA* **104:** 15424–15429.

Crepin, V.F., Girard, F., Schuller, S., Phillips, A.D., Mousnier, A., and Frankel, G. (2010) Dissecting the role of the Tir:Nck and Tir:IRTKS/IRSp53 signalling pathways *in vivo*. *Mol Microbiol* **75:** 308–323.

Croxen, M.A., and Finlay, B.B. (2010) Molecular mechanisms of *Escherichia coli* pathogenicity. *Nat Rev Microbiol* **8:** 26–38.

Dean-Nystrom, E.A., Bosworth, B.T., and Moon, H.W. (1999) Pathogenesis of *Escherichia coli* O157:H7 in weaned calves. *Adv Exp Med Biol* **473:** 173–177.

Deng, W., Vallance, B.A., Li, Y., Puente, J.L., and Finlay, B.B. (2003) *Citrobacter rodentium* translocated intimin receptor (Tir) is an essential virulence factor needed for actin condensation, intestinal colonization and colonic hyperplasia in mice. *Mol Microbiol* **48:** 95–115.

Deng, W., Puente, J.L., Gruenheid, S., Li, Y., Vallance, B.A., Vazquez, A., *et al*. (2004) Dissecting virulence: systematic

and functional analyses of a pathogenicity island. *Proc Natl Acad Sci USA* **101:** 3597–3602.

Donnenberg, M.S., Tacket, C.O., James, S.P., Losonsky, G., Nataro, J.P., Wasserman, S.S., *et al*. (1993) Role of the *eaeA* gene in experimental enteropathogenic *Escherichia coli* infection. *J Clin Invest* **92:** 1412–1417.

Frankel, G., and Phillips, A.D. (2008) Attaching effacing *Escherichia coli* and paradigms of Tir-triggered actin polymerization: getting off the pedestal. *Cell Microbiol* **10:** 549–556.

Garmendia, J., Phillips, A.D., Carlier, M.F., Chong, Y., Schuller, S., Marches, O., *et al*. (2004) TccP is an enterohaemorrhagic *Escherichia coli* O157:H7 type III effector protein that couples Tir to the actin-cytoskeleton. *Cell Microbiol* **6:** 1167–1183.

Garmendia, J., Frankel, G., and Crepin, V.F. (2005) Enteropathogenic and enterohemorrhagic *Escherichia coli* infections: translocation, translocation, translocation. *Infect Immun* **73:** 2573–2585.

Ghaem-Maghami, M., Simmons, C.P., Daniell, S., Pizza, M., Lewis, D., Frankel, G., and Dougan, G. (2001) Intimin-specific immune responses prevent bacterial colonization by the attaching-effacing pathogen *Citrobacter rodentium*. *Infect Immun* **69:** 5597–5605.

Girard, F., Crepin, V.F., and Frankel, G. (2009) Modelling of infection by enteropathogenic *Escherichia coli* strains in lineages 2 and 4 *ex vivo* and *in vivo* by using *Citrobacter rodentium* expressing TccP. *Infect Immun* **77:** 1304–1314.

Gobius, K.S., Higgs, G.M., and Desmarchelier, P.M. (2003) Presence of activatable Shiga toxin genotype (stx2d) in Shiga toxigenic *Escherichia coli* from livestock sources. *J Clin Microbiol* **41:** 3777–3783.

Goldberg, M.B. (2001) Actin-based motility of intracellular microbial pathogens. *Microbiol Mol Biol Rev* **65:** 595–626, table of contents.

de Grado, M., Abe, A., Gauthier, A., Steele-Mortimer, O., DeVinney, R., and Finlay, B.B. (1999) Identification of the intimin-binding domain of Tir of enteropathogenic *Escherichia coli*. *Cell Microbiol* **1:** 7–17.

Gruenheid, S., DeVinney, R., Bladt, F., Goosney, D., Gelkop, S., Gish, G.D., *et al*. (2001) Enteropathogenic *E. coli* Tir binds Nck to initiate actin pedestal formation in host cells. *Nat Cell Biol* **3:** 856–859.

Guttman, J.A., Samji, F.N., Li, Y., Vogl, A.W., and Finlay, B.B. (2006) Evidence that tight junctions are disrupted due to intimate bacterial contact and not inflammation during attaching and effacing pathogen infection *in vivo*. *Infect Immun* **74:** 6075–6084.

Hanajima-Ozawa, M., Matsuzawa, T., Fukui, A., Kamitani, S., Ohnishi, H., Abe, A., *et al*. (2007) Enteropathogenic *Escherichia coli*, *Shigella flexneri*, and *Listeria monocytogenes* recruit a junctional protein, zonula occludens-1, to actin tails and pedestals. *Infect Immun* **75:** 565–573.

Hartland, E.L., Batchelor, M., Delahay, R.M., Hale, C., Matthews, S., Dougan, G., *et al*. (1999) Binding of intimin from enteropathogenic *Escherichia coli* to Tir and to host cells. *Mol Microbiol* **32:** 151–158.

Hayward, R.D., Leong, J.M., Koronakis, V., and Campellone, K.G. (2006) Exploiting pathogenic *Escherichia coli* to model transmembrane receptor signalling. *Nat Rev Microbiol* **4:** 358–370.

Holmes, A., Muhlen, S., Roe, A.J., and Dean, P. (2010) The EspF effector, a bacterial pathogen's Swiss army knife. *Infect Immun* **78:** 4445–4453.

Kamada, N., Kim, Y.G., Sham, H.P., Vallance, B.A., Puente, J.L., Martens, E.C., and Nunez, G. (2012) Regulated virulence controls the ability of a pathogen to compete with the gut microbiota. *Science* **336:** 1325–1329.

Kaper, J.B., Nataro, J.P., and Mobley, H.L. (2004) Pathogenic *Escherichia coli*. *Nat Rev Microbiol* **2:** 123–140.

Karmali, M.A., Gannon, V., and Sargeant, J.M. (2009) Verocytotoxin-producing *Escherichia coli* (VTEC). *Vet Microbiol* **140:** 360–370.

Keepers, T.R., Psotka, M.A., Gross, L.K., and Obrig, T.G. (2006) A murine model of HUS: Shiga toxin with lipopolysaccharide mimics the renal damage and physiologic response of human disease. *J Am Soc Nephrol* **17:** 3404–3414.

Kenny, B. (1999) Phosphorylation of tyrosine 474 of the enteropathogenic *Escherichia coli* (EPEC) Tir receptor molecule is essential for actin nucleating activity and is preceded by additional host modifications. *Mol Microbiol* **31:** 1229–1241.

Kenny, B., DeVinney, R., Stein, M., Reinscheid, D.J., Frey, E.A., and Finlay, B.B. (1997) Enteropathogenic *E. coli* (EPEC) transfers its receptor for intimate adherence into mammalian cells. *Cell* **91:** 511–520.

Lommel, S., Benesch, S., Rottner, K., Franz, T., Wehland, J., and Kuhn, R. (2001) Actin pedestal formation by enteropathogenic *Escherichia coli* and intracellular motility of *Shigella flexneri* are abolished in N-WASP-defective cells. *EMBO Rep* **2:** 850–857.

Lyubimova, A., Garber, J.J., Upadhyay, G., Sharov, A., Anastasoaie, F., Yajnik, V., *et al*. (2010) Neural Wiskott-Aldrich syndrome protein modulates Wnt signaling and is required for hair follicle cycling in mice. *J Clin Invest* **120:** 446–456.

McDaniel, T.K., Jarvis, K.G., Donnenberg, M.S., and Kaper, J.B. (1995) A genetic locus of enterocyte effacement conserved among diverse enterobacterial pathogens. *Proc Natl Acad Sci USA* **92:** 1664–1668.

McNamara, B.P., Koutsouris, A., O'Connell, C.B., Nougayrede, J.P., Donnenberg, M.S., and Hecht, G. (2001) Translocated EspF protein from enteropathogenic *Escherichia coli* disrupts host intestinal barrier function. *J Clin Invest* **107:** 621–629.

Mallick, E.M., Brady, M.J., Luperchio, S.A., Vanguri, V., Magoun, L., Liu, H., *et al*. (2012a) Allele- and Tir-independent functions of intimin in diverse animal infection models. *Front Microbiol* **3:** 11.

Mallick, E.M., McBee, M.E., Vanguri, V.K., Melton-Celsa, A.R., Schlieper, K., Karalius, B.J., *et al*. (2012b) A novel murine infection model for Shiga toxin-producing *Escherichia coli*. *J Clin Invest* **122:** 4012–4024.

Marches, O., Nougayrede, J.P., Boullier, S., Mainil, J., Charlier, G., Raymond, I., *et al*. (2000) Role of Tir and intimin in the virulence of rabbit enteropathogenic *Escherichia coli* serotype O103:H2. *Infect Immun* **68:** 2171–2182.

Marches, O., Wiles, S., Dziva, F., La Ragione, R.M., Schuller,

S., Best, A., *et al*. (2005) Characterization of two non-locus of enterocyte effacement-encoded type III-translocated effectors, NleC and NleD, in attaching and effacing pathogens. *Infect Immun* **73:** 8411–8417.

el Marjou, F., Janssen, K.P., Chang, B.H., Li, M., Hindie, V., Chan, L., *et al*. (2004) Tissue-specific and inducible Cre-mediated recombination in the gut epithelium. *Genesis* **39:** 186–193.

Melton-Celsa, A., Mohawk, K., Teel, L., and O'Brien, A. (2011) Pathogenesis of Shiga-toxin producing *Escherichia coli*. *Curr Top Microbiol Immunol* **357:** 67–103.

Mohawk, K.L., and O'Brien, A.D. (2011) Mouse models of *Escherichia coli* O157:H7 infection and Shiga toxin injection. *J Biomed Biotechnol* **2011:** 258185.

Moon, H.W., Whipp, S.C., Argenzio, R.A., Levine, M.M., and Giannella, R.A. (1983) Attaching and effacing activities of rabbit and human enteropathogenic *Escherichia coli* in pig and rabbit intestines. *Infect Immun* **41:** 1340–1351.

Mundy, R., Petrovska, L., Smollett, K., Simpson, N., Wilson, R.K., Yu, J., *et al*. (2004) Identification of a novel *Citrobacter rodentium* type III secreted protein, EspI, and roles of this and other secreted proteins in infection. *Infect Immun* **72:** 2288–2302.

Nagano, K., Taguchi, K., Hara, T., Yokoyama, S., Kawada, K., and Mori, H. (2003) Adhesion and colonization of enterohemorrhagic *Escherichia coli* O157:H7 in cecum of mice. *Microbiol Immunol* **47:** 125–132.

Nakao, H., and Takeda, T. (2000) *Escherichia coli* Shiga toxin. *J Nat Toxins* **9:** 299–313.

Nart, P., Naylor, S.W., Huntley, J.F., McKendrick, I.J., Gally, D.L., and Low, J.C. (2008) Responses of cattle to gastrointestinal colonization by *Escherichia coli* O157:H7. *Infect Immun* **76:** 5366–5372.

Nougayrede, J.P., Fernandes, P.J., and Donnenberg, M.S. (2003) Adhesion of enteropathogenic *Escherichia coli* to host cells. *Cell Microbiol* **5:** 359–372.

Obrig, T.G. (2010) *Escherichia coli* Shiga toxin mechanisms of action in renal disease. *Toxins (Basel)* **2:** 2769–2794.

Ogura, Y., Ooka, T., Whale, A., Garmendia, J., Beutin, L., Tennant, S., *et al*. (2007) TccP2 of O157:H7 and non-O157 enterohemorrhagic *Escherichia coli* (EHEC): challenging the dogma of EHEC-induced actin polymerization. *Infect Immun* **75:** 604–612.

Pennington, H. (2010) *Escherichia coli* O157. *Lancet* **376:** 1428–1435.

Peralta-Ramirez, J., Hernandez, J.M., Manning-Cela, R., Luna-Munoz, J., Garcia-Tovar, C., Nougayrede, J.P., *et al*. (2008) EspF interacts with nucleation-promoting factors to recruit junctional proteins into pedestals for pedestal maturation and disruption of paracellular permeability. *Infect Immun* **76:** 3854–3868.

Phillips, N., Hayward, R.D., and Koronakis, V. (2004) Phosphorylation of the enteropathogenic *E. coli* receptor by the Src-family kinase c-Fyn triggers actin pedestal formation. *Nat Cell Biol* **6:** 618–625.

Pierard, D., De Greve, H., Haesebrouck, F., and Mainil, J. (2012) O157:H7 and O104:H4 Vero/Shiga toxin-producing *Escherichia coli* outbreaks: respective role of cattle and humans. *Vet Res* **43:** 13.

Psotka, M.A., Obata, F., Kolling, G.L., Gross, L.K., Saleem, M.A., Satchell, S.C., *et al*. (2009) Shiga toxin 2 targets the murine renal collecting duct epithelium. *Infect Immun* **77:** 959–969.

Rasko, D.A., Webster, D.R., Sahl, J.W., Bashir, A., Boisen, N., Scheutz, F., *et al*. (2011) Origins of the *E. coli* strain causing an outbreak of hemolytic-uremic syndrome in Germany. *N Engl J Med* **365:** 709–717.

Ritchie, J.M., and Waldor, M.K. (2005) The locus of enterocyte effacement-encoded effector proteins all promote enterohemorrhagic *Escherichia coli* pathogenicity in infant rabbits. *Infect Immun* **73:** 1466–1474.

Ritchie, J.M., Thorpe, C.M., Rogers, A.B., and Waldor, M.K. (2003) Critical roles for stx2, *eae*, and *tir* in enterohemorrhagic *Escherichia coli*-induced diarrhea and intestinal inflammation in infant rabbits. *Infect Immun* **71:** 7129–7139.

Ritchie, J.M., Brady, M.J., Riley, K.N., Ho, T.D., Campellone, K.G., Herman, I.M., *et al*. (2008) $EspF_U$, a type III-translocated effector of actin assembly, fosters epithelial association and late-stage intestinal colonization by *E. coli* O157:H7. *Cell Microbiol* **10:** 836–847.

Rivera, G.M., Briceno, C.A., Takeshima, F., Snapper, S.B., and Mayer, B.J. (2004) Inducible clustering of membrane-targeted SH3 domains of the adaptor protein Nck triggers localized actin polymerization. *Curr Biol* **14:** 11–22.

Robinson, C.M., Sinclair, J.F., Smith, M.J., and O'Brien, A.D. (2006) Shiga toxin of enterohemorrhagic *Escherichia coli* type O157:H7 promotes intestinal colonization. *Proc Natl Acad Sci USA* **103:** 9667–9672.

Rohatgi, R., Nollau, P., Ho, H.Y., Kirschner, M.W., and Mayer, B.J. (2001) Nck and phosphatidylinositol 4,5-bisphosphate synergistically activate actin polymerization through the N-WASP-Arp2/3 pathway. *J Biol Chem* **276:** 26448–26452.

Sanger, J.M., Chang, R., Ashton, F., Kaper, J.B., and Sanger, J.W. (1996) Novel form of actin-based motility transports bacteria on the surfaces of infected cells. *Cell Motil Cytoskeleton* **34:** 279–287.

Sauter, K.A., Melton-Celsa, A.R., Larkin, K., Troxell, M.L., O'Brien, A.D., and Magun, B.E. (2008) Mouse model of hemolytic-uremic syndrome caused by endotoxin-free Shiga toxin 2 (Stx2) and protection from lethal outcome by anti-Stx2 antibody. *Infect Immun* **76:** 4469–4478.

Schauer, D.B., and Falkow, S. (1993a) Attaching and effacing locus of a *Citrobacter freundii* biotype that causes transmissible murine colonic hyperplasia. *Infect Immun* **61:** 2486–2492.

Schauer, D.B., and Falkow, S. (1993b) The *eae* gene of *Citrobacter freundii* biotype 4280 is necessary for colonization in transmissible murine colonic hyperplasia. *Infect Immun* **61:** 4654–4661.

Scheiring, J., Andreoli, S.P., and Zimmerhackl, L.B. (2008) Treatment and outcome of Shiga-toxin-associated hemolytic uremic syndrome (HUS). *Pediatr Nephrol* **23:** 1749–1760.

Schmidt, H. (2001) Shiga-toxin-converting bacteriophages. *Res Microbiol* **152:** 687–695.

Schuller, S. (2011) Shiga toxin interaction with human intestinal epithelium. *Toxins (Basel)* **3:** 626–639.

Schuller, S., Chong, Y., Lewin, J., Kenny, B., Frankel, G., and Phillips, A.D. (2007a) Tir phosphorylation and Nck/N-WASP recruitment by enteropathogenic and enterohaemorrhagic *Escherichia coli* during *ex vivo* coloni-

zation of human intestinal mucosa is different to cell culture models. *Cell Microbiol* **9:** 1352–1364.
Schuller, S., Heuschkel, R., Torrente, F., Kaper, J.B., and Phillips, A.D. (2007b) Shiga toxin binding in normal and inflamed human intestinal mucosa. *Microbes Infect* **9:** 35–39.
Shaner, N.C., Sanger, J.W., and Sanger, J.M. (2005) Actin and alpha-actinin dynamics in the adhesion and motility of EPEC and EHEC on host cells. *Cell Motil Cytoskeleton* **60:** 104–120.
Sherman, P.M., and Boedeker, E.C. (1987) Regional differences in attachment of enteroadherent *Escherichia coli* strain RDEC-1 to rabbit intestine: luminal colonization but lack of mucosal adherence in jejunal self-filling blind loops. *J Pediatr Gastroenterol Nutr* **6:** 439–444.
Simmons, C.P., Clare, S., Ghaem-Maghami, M., Uren, T.K., Rankin, J., Huett, A., *et al*. (2003) Central role for B lymphocytes and CD4+ T cells in immunity to infection by the attaching and effacing pathogen *Citrobacter rodentium*. *Infect Immun* **71:** 5077–5086.
Snapper, S.B., Takeshima, F., Anton, I., Liu, C.H., Thomas, S.M., Nguyen, D., *et al*. (2001) N-WASP deficiency reveals distinct pathways for cell surface projections and microbial actin-based motility. *Nat Cell Biol* **3:** 897–904.
Srikanth, C.V., Wall, D.M., Maldonado-Contreras, A., Shi, H.N., Zhou, D., Demma, Z., *et al*. (2010) *Salmonella* pathogenesis and processing of secreted effectors by caspase-3. *Science* **330:** 390–393.
Swimm, A., Bommarius, B., Li, Y., Cheng, D., Reeves, P., Sherman, M., *et al*. (2004) Enteropathogenic *E. coli* use redundant tyrosine kinases to form actin pedestals. *Mol Biol Cell* **15:** 3520–3529.
Tarr, P.I., Gordon, C.A., and Chandler, W.L. (2005) Shiga-toxin-producing *Escherichia coli* and haemolytic uraemic syndrome. *Lancet* **365:** 1073–1086.
Tzipori, S., Gunzer, F., Donnenberg, M.S., de Montigny, L., Kaper, J.B., and Donohue-Rolfe, A. (1995) The role of the *eaeA* gene in diarrhea and neurological complications in a gnotobiotic piglet model of enterohemorrhagic *Escherichia coli* infection. *Infect Immun* **63:** 3621–3627.
Vallance, B.A., Deng, W., Knodler, L.A., and Finlay, B.B. (2002) Mice lacking T and B lymphocytes develop transient colitis and crypt hyperplasia yet suffer impaired bacterial clearance during *Citrobacter rodentium* infection. *Infect Immun* **70:** 2070–2081.
Vingadassalom, D., Campellone, K.G., Brady, M.J., Skehan, B., Battle, S.E., Robbins, D., *et al*. (2010) Enterohemorrhagic *E. coli* requires N-WASP for efficient type III translocation but not for $EspF_U$-mediated actin pedestal formation. *PLoS Pathog* **6:** e1001056.
Vlisidou, I., Dziva, F., La Ragione, R.M., Best, A., Garmendia, J., Hawes, P., *et al*. (2006) Role of intimin-tir interactions and the tir-cytoskeleton coupling protein in the colonization of calves and lambs by *Escherichia coli* O157:H7. *Infect Immun* **74:** 758–764.
Wales, A.D., Pearson, G.R., Skuse, A.M., Roe, J.M., Hayes, C.M., Cookson, A.L., and Woodward, M.J. (2001) Attaching and effacing lesions caused by *Escherichia coli* O157:H7 in experimentally inoculated neonatal lambs. *J Med Microbiol* **50:** 752–758.
Whale, A.D., Garmendia, J., Gomes, T.A., and Frankel, G. (2006) A novel category of enteropathogenic *Escherichia coli* simultaneously utilizes the Nck and TccP pathways to induce actin remodelling. *Cell Microbiol* **8:** 999–1008.
Whitehead, R.H., and Robinson, P.S. (2009) Establishment of conditionally immortalized epithelial cell lines from the intestinal tissue of adult normal and transgenic mice. *Am J Physiol Gastrointest Liver Physiol* **296:** G455–G460.
Wiles, S., Clare, S., Harker, J., Huett, A., Young, D., Dougan, G., and Frankel, G. (2004) Organ specificity, colonization and clearance dynamics *in vivo* following oral challenges with the murine pathogen *Citrobacter rodentium*. *Cell Microbiol* **6:** 963–972.

Supporting information

Additional Supporting Information may be found in the online version of this article at the publisher's web-site:

Fig. S1. Mice with intestine-specific N-WASP deletion exhibit normal intestinal histology and lack spontaneous inflammation. H&E staining of colon (top row) and ileum (second row) reveals normal crypt-villous morphology, and the presence of organized columnar epithelium containing enterocytes and goblet cells without inflammatory cell infiltrate. Alcian blue staining (third row) indicates the presence of normal numbers of goblet cells in iNWKO and wild type mice. Higher power H&E (bottom row) of small intestine crypts reveals the presence of normal numbers of Paneth cells in iNWKO mice.

Fig. S2. iNWKO and littermate control mice are equally susceptible to infection by *Salmonella*.

A–D. iNWKO (green circles) and littermate control (black squares) mice were infected with approximately 1.6×10^8 cfu *Salmonella* and faecal (A), liver (B), splenic (C), and colonic (D) colonization were measured at 48 h post-infection. Shown are the average cfu g^{-1} faeces or cfu mg^{-1} tissue ± SEM. Data are representative of one of two independent experiments using two to seven mice per group. Note that no significant differences between iNWKO and littermate control mice were detected.

E. H&E-stained histological sections of liver, spleen, and colon from iNWKO and littermate control mice infected with *Salmonella* at 48 h post-infection. Magnification is 100× for liver and spleen sections and 200× for colon sections. Scale bars measure 100 μm.

Fig. S3. N-WASP promotes high-level colonization and body weight loss during *C. rodentium* (Φstx_{2dact}) infection.

A. Colonization of iNWKO (green) or littermate controls (black) mice infected with *C. rodentium* (Φstx_{2dact}) was determined by viable counts in stool samples. Shown are the average cfu (± SEM) of three iNWKO and two littermate controls. Data are representative of one of four single experiments using two to seven mice per group. Statistically significant differences between the two groups were determined by two-way ANOVA and Bonferroni post-tests and in the experiment shown no statistically significant differences were identified.

B. Per cent body weight loss during infection of iNWKO (green) or littermate control (black) mice infected with *C. rodentium* (Φstx_{2dact}) was determined. Shown are the averages (± SEM) of six iNWKO and seven littermate control mice per group. Data are one representative of four independent experiments using two to seven mice per group. Statistically significant differences

between the two groups were determined by two-way ANOVA and Bonferroni post-tests and in the experiment shown no statistically significant differences were identified.

Fig. S4. *C. rodentium* harbouring pTir$_{WT}$ or pTir$_{Y471F}$ produce and secrete similar levels of Tir. Western blots of Tir from isogenic strains of *C. rodentium*, and *C. rodentium* (Φ*stx*$_{2dact}$), showing (A, B) wild type *C. rodentium*, *C. rodentium*Δ*tir*, *C. rodentium*Δ*tir*/Tir$_{WT}$, and *C. rodentium*Δ*tir*/pTir$_{Y471F}$ mutants and (C, D) wild type *C. rodentium* (Φ*stx*$_{2dact}$), *C. rodentium* (Φ*stx*$_{2dact}$)Δ*tir, C. rodentium* (Φ*stx*$_{2dact}$)Δ*tir*/pTir$_{WT}$, and *C. rodentium* (Φ*stx*$_{2dact}$)Δ*tir*/pTir$_{Y471F}$ mutants. All membranes were blotted with anti-*C. rodentium* Tir antibody. Despite its predicted molecular weight of 56.2 kD, *C. rodentium* Tir migrates at approximately 68 kDa (Deng *et al*., 2003), likely in part due to proposed post-translational modifications (Kenny *et al*., 1997; DeVinney *et al*., 1999).
A and C. TCA-precipitated culture supernatants of indicated strains. SDS-PAGE loading was standardized to protein concentration as determined by nanodrop at an absorbance of 280 nm.
B and D. Bacterial lysates of indicated strains. Lanes were loaded with approximately equal amounts of lysate, based on OD_{600} culture readings. All membranes were blotted with anti-*C. rodentium* Tir antibody. The asterisk (*) indicates an unknown cross-reacting band.

Fig. S5. TirY471F does not promote *C. rodentium* (Φ*stx*$_{2dact}$) pedestal formation on cultured cells.
A. Mouse embryonic fibroblasts (MEFs) were infected with the indicated *C. rodentium* strains and the number of bound bacteria per cell was counted for four sets of 25 randomly selected cells. The experiment was performed in triplicate. Shown in the box is the mean number of bacteria per cell ± SEM.
B. MEFs were infected with isogenic strains of *C. rodentium* in a FAS assay. Bacteria and MEF cell nuclei were stained with DAPI (blue) and F-actin was stained with phalloidin (red).

Table S1. Bacterial and phage strains used in this study.

Table S2. Plasmids used in this study.

Table S3. Oligonucleotide primers used in this study.

Table S4. *C. rodentium* pTir and pTir$_{Y471F}$ are stable during mouse infection.